

1 **Spatial-temporal changes in flow hydraulic characteristics and soil loss**
2 **during gully headcut erosion under controlled conditions**

3
4 Mingming Guo^a, Zhuoxin Chen^b, Wenlong Wang^{b,c*}, Tianchao Wang^d, Qianhua Shi^b, Hongliang
5 Kang^b, Man Zhao^b, Lanqian Feng^c

6
7 a Key laboratory of Mollisols Agroecology, Northeast Institute of Geography and Agroecology,
8 Chinese Academy of Sciences, Harbin 150081, Heilongjiang, China

9 b State Key Laboratory of Soil Erosion and Dryland Farming on the Loess Plateau, Institute of Water
10 and Soil Conservation, Northwest A&F University, Yangling, Shaanxi 712100, China

11 c Institute of Soil and Water Conservation, Chinese Academy of Sciences and Ministry of Water
12 Resources, Yangling, Shaanxi 712100, China

13 d Ulanyab Grassland Station, Jining, Inner Mongolia 012000, China

14 ***Corresponding author:** Wenlong Wang

15 E-mail addresses: nwafu_wwl@163.com; wllwang@nwsuaf.edu.cn

16

17 **Abstract**

18 The temporal-spatial changes in flow hydraulics and energy consumption and their associated soil
19 erosion remain unclear during gully headcut retreat. A simulated scouring experiment was conducted
20 on five headcut plots consisting of upstream area (UA), gully headwall (GH) and gully bed (GB) to
21 elucidate the temporal-spatial changes in flow hydraulic, energy consumption, and soil loss during
22 headcut erosion. The flow velocity at the brink of headcut increased as a power function of time,
23 whereas the jet velocity entry to plunge pool and jet shear stress logarithmically or linearly decreased
24 over time. The jet properties were significantly affected by upstream flow discharge. The Reynold
25 number, runoff shear stress, and stream power of UA and GB increased as logarithmic or power
26 functions of time, but the Froude number decreased logarithmically over time. The Reynold number,
27 shear stress and stream power decreased by 56.0%, 63.8% and 55.9%, respectively, but the Froude
28 number increased by 7.9% when flow dropped from UA to GB. The accumulated energy consumption
29 of UA, GH and GB positions linearly increased with time. 91.12% - 99.90% of total flow energy was
30 consumed during headcut erosion, of which the gully head accounted for 77.7% of total energy
31 dissipation followed by UA (18.3%) and GB (4.0%). The soil loss rate of the “UA-GH-GB” system
32 initially rose and then gradually declined and levelled off. The soil loss of UA and GH decreased
33 logarithmically over time, whereas the GB was mainly characterized by sediment deposition. The
34 proportion of soil loss at UA and GH are 11.5% and 88.5%, respectively, of which the proportion of
35 deposited sediment on GB reached 3.8%. The change in soil loss of UA, GH and GB was significantly
36 affected by flow hydraulic and jet properties. The critical energy consumption initiating soil erosion
37 of UA, GH, and GB are 1.62 J s^{-1} , 5.79 J s^{-1} and 1.64 J s^{-1} , respectively. These results are helpful to
38 deepen the understanding of gully erosion process and hydrodynamic mechanism and also can provide
39 scientific basis for the construction of gully erosion model and the design of gully erosion prevention
40 measures.

41
42 **Keywords:** Gully erosion; Hydraulic property; Headcut retreat; Mass failure; Energy dissipation

43

44 **1 Introduction**

45 Gully erosion is a typical soil erosion process whereby concentrated runoff from an upstream
46 drainage area recurs in a channel and erodes soil from the area through which runoff passed to
47 considerable depth (Poesen et al., 2003; Zhu, 2012). Gully erosion is recognized as the main sediment
48 source in some hilly and gully-dominated watersheds (Poesen et al., 2003; Valentin et al., 2005;
49 Dotterweich et al., 2012). Poesen et al. (2003) reported that soil loss amount caused by gully erosion
50 accounts for 10% - 94% of total soil loss amount based on the collected data from published articles.
51 Moreover, gully erosion can severely damage to infrastructure, enhance the terrain fragmentation, and
52 cause ecosystem instability, land degradation and food safety (Vanmaercke et al, 2016; Zhang et al.,
53 2018; Hosseinalizadeh et al., 2019; Arabameri et al., 2020; Bogale et al., 2020; Belayneh et al., 2020;
54 Wen et al., 2020).

55 As the primary process of the gully erosion, the gully headcut retreat often significantly influences
56 and determines gully erosion (Oostwoud-Wijdenes et al., 2000; Vandekerckhove et al., 2003; Guo et
57 al., 2019). A headcut is defined as a vertical or near-vertical drop or discontinuity on the bed of a gully
58 occurring where flow is concentrated at a knickpoint (Hanson et al., 2001; Bennett et al., 2000). Many
59 studies have demonstrated that the gully erosion is the result of the combined actions of plunge pool
60 erosion by jet flow, upstream runoff incision, headwall erosion by on-wall flow, mass failure of gully
61 head and wall collapse (Vanmaercke et al., 2016; Addisie et al., 2017; Guo et al., 2019). Once a headcut
62 is formed in upstream area, the gully will develop rapidly and not stop forward until a critical
63 topographic condition is formed ($S \leq a \cdot A^b$, where S and A is the slope gradient and drainage area
64 upstream gully headcut, respectively) (Kirkby et al., 2003). Moreover, the different landform units
65 (upstream area, UA; gully head, GH; gully bed, GB) of gully system exhibited completely different
66 erosion processes and hydrodynamic mechanisms during gully headcut erosion (Zhang et al., 2018;
67 Guo et al., 2019; Shi et al., 2020a). The combination and interaction of erosion processes of the three
68 landform units determined gully headcut erosion process (Vanmaercke et al., 2016). Therefore,
69 clarifying the soil erosion process and characteristics of the three landform units is critical to
70 systematically and clearly reveal the mechanism of gully headcut erosion.

71 Previous studies suggested that gully heacut erosion is affected by various factors including

72 topography, land use change, vegetation, soil properties, and climate (Vanwallegem et al., 2003;
73 Ionita, 2006; Rodzik et al., 2009; Rieke-Zapp and Nichols, 2011; Torri and Poesen, 2014; Ionita et al.,
74 2015; Vannoppen et al., 2015; Guo et al., 2019, 2020a). In terms of topography, most of studies focused
75 on the threshold relationship ($S \leq a \cdot A^b$) to initiate gully erosion (e.g., Torri and Poesen, 2014). Several
76 experimental studies demonstrated that the upstream slope gradient and headcut height have significant
77 effects on headcut erosion (e.g., Bennett, 1999; Zhang et al., 2018). Land use change is recognized as
78 having the strongest effect on processes related to gully erosion (Poesen et al., 2003; Chaplot et al.,
79 2005; Descroix et al., 2008), and also significantly affects the activation of gully headcut erosion (e.g.,
80 Torri and Poesen, 2014). In this aspect, the vegetation coverage is a parameter that is often used to
81 clarify its effect on gully erosion (e.g., De Baets et al., 2007; Martínez-Casasnovas et al., 2009),
82 however, in fact, the vegetation effect mainly depends on the root characteristics and its distribution at
83 gully head (e.g., Vannoppen et al., 2015; Guo et al., 2019). Nevertheless, at present, the most of studies
84 on gully erosion focus on the changes in gully morphology between different periods at a watershed
85 or regional scale (Vanmaercke et al., 2016), which is why the previous studies fail to address the effects
86 of root systems on gully headcut retreat. Guo et al. (2019) concluded that the grass (*Agropyron*
87 *cristatum*) could reduce soil loss and headcut retreat distance by 45.6 - 68.5%, 66.9 - 85.4%,
88 respectively, compared with bare land, and the roots of 0 - 0.5 mm in diameter showed the greatest
89 controlling influence on headcut erosion. In terms of soil properties, lots of studies have proved the
90 significant effect of soil properties on gully headcut erosion (e.g., Nazari Samani et al., 2010), which
91 is mainly related to the change in soil erodibility induced by soil properties including soil texture, soil
92 vertical joints, soluble mineral content, soil lithology, and physicochemical properties (Sanchis et al.,
93 2008; Vanmaercke et al., 2016; Guo et al., 2020a). Rainfall, the main climate factor, is closely related
94 to runoff generation and thus be expected to affect headcut erosion. Many studies have reported that
95 the initiation of gully headcut is correlated with rainfall characteristics (e.g., summation of rainfall
96 from 24-hour rains equal to or greater than 0.5 inches) (Beer and Johnson, 1963; Vandekerckhove et
97 al., 2003; Rieke-Zapp and Nichols, 2011). However, the great difference in the threshold value relating
98 to rainfall factors was found among different areas of the world due to fully different erosion
99 environments. For example, in the northeast of China, the gully erosion is the result of soil thawing,

100 rainfall runoff and snowmelt runoff (Li et al., 2016b; Xu et al., 2019). Furthermore, at present, the
101 most of studies on gully erosion were conducted to quantify the change in gully erosion (retreat rate,
102 area and volume) at different spatial and temporal scales by using remote sensing interpretation, real-
103 time monitoring and meta-analysis based on literature data (e.g., Vanmaercke et al., 2016). However,
104 the influencing mechanism of these factors on gully headcut erosion is still unclear and need to be
105 revealed in future studies.

106 Evidently, the concentrated flow upstream gully head, mainly depended on the drainage area
107 upstream gully heads and rainfall characteristics, is the main and original drive force triggering headcut
108 erosion. The runoff firstly eroded the upstream area and then was parted into two types of flow (on-
109 wall flow and jet flow) at the brinkpoint of gully headcut (Guo et al., 2021a). Consequently, the on-
110 wall flow persistently eroded headwall soil, and the jet flow violently impacted gully bed soil and
111 formed a plunge pool (Su et al., 2015; Guo et al., 2019). Subsequently, the two types of flow merged
112 again and eroded gully bed together (Zhang et al., 2018; Shi et al., 2020a). The runoff hydraulic or jet
113 flow properties at different landform units (UA, GH and GB) are significantly different, which is an
114 important reason for the difference in erosion process among different landform units. However, the
115 temporal-spatial change in runoff and jet properties during headcut erosion is still unclear and thus
116 needs to be clarified. Furthermore, at present, some experimental studies on headcut erosion of rill,
117 ephemeral gully, gully and bank gully were conducted to investigate the runoff properties, energy
118 consumption, sediment transport process, morphology evolution and empirical model (Bennett and
119 Casali, 2001; Wells et al., 2009a, 2009b; Su et al., 2014; Xu et al., 2017a; Guo et al., 2019; Shi et al.,
120 2020a). However, relatively few knowledges were obtained to systemically reveal the hydrodynamic
121 mechanism of gully headcut erosion. Therefore, elucidating the temporal-spatial changes in runoff
122 hydraulic and soil loss and hydrodynamic mechanism of UA, GH and GB is of great importance to
123 systematically reveal the hydrodynamics mechanism of gully headcut erosion.

124 Given the above-mentioned issues, a series of simulated gully headcut erosion experiments
125 subjected to inflow scouring are conducted to (1) investigate the temporal-spatial change in runoff
126 hydraulic and jet flow properties during headcut erosion, (2) quantify the dynamic change of energy
127 consumption and soil loss and their spatial distribution, and (3) reveal the erosion hydrodynamic

128 mechanism of UA, GH and GB.

129 **2 Materials and Methods**

130 **2.1 Study area**

131 This experiment was carried out at the Xifeng Soil and Water Conservation Experimental Station
132 that is located in the Nanxiaohegou watershed, Qingyang City, Gansu Province, China. The study area
133 belongs to a semi-arid continental climate with a mean annual temperature of 9.3 °C. The mean annual
134 precipitation is 546.8 mm (1954 - 2014), of which precipitation from May to September accounts for
135 76.9% of the total precipitation (Xia et al., 2017; Guo et al., 2019). The elevation ranges from 1050 to
136 1423 m. The main landforms include gentle loess-tableland, steep hillslope and gully channel, and
137 their areas account for 57.0%, 15.7% and 27.3%, respectively. The loess-tableland is characterized by
138 low slope (1 - 5°), gentle and flat terrain and fertile soil. The main soil type is loessial soil with silt
139 loam texture. Most of hillslopes have been constructed as slope-terraces. The main gully channel is
140 usually U-shaped and the branch-gully is more actively developed and easily eroded as a V-shaped by
141 runoff from loess-tableland (Xu et al., 2019). The flat loess-tableland can accumulate the 67.4% of
142 total runoff and cause serious gully erosion that can contribute 86.3% of the total soil erosion (Guo et
143 al., 2019). The original plant species have been seriously destroyed. Since the 1970s, the “Three
144 Protection Belts” system, the “Four Eco-Economical Belts” system and the “Grain for Green” project
145 (Zhao, 1994; Fu et al., 2011) were implemented to control soil erosion. The main land use on loess-
146 tableland position has always been farmland and orchards, while the land use on hillslope is sloping
147 farmland and orchards before 1999, which have been changed into forested and grassy land due to the
148 “Grain for Green” project. The current mean annual soil erosion rate has been reduced to 4350 Mg km⁻²
149 y⁻¹ in the study watershed (Guo et al., 2019). The plants are primarily artificially planted arbors and
150 herbaceous vegetation and shrubs (Guo et al., 2021b).

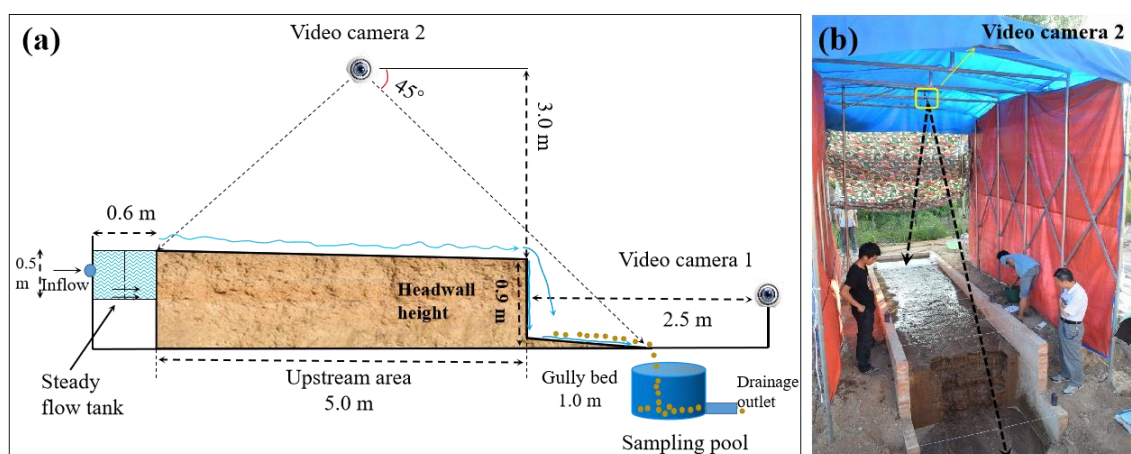
151

152 **2.2 Experimental design**

153 **2.2.1 Gully head experimental plot construction**

154 Five gully head plots for headcut erosion experiments were constructed at the experimental station
155 in April 2018. Fig. 1 shows the basic information of the gully head plot consisting of three landform

156 units (upstream area, headwall and gully bed). The plot width and slope gradient of upstream area and
 157 gully bed are uniformly designed as 1.5 m and 3° , respectively. The upstream area length, the height
 158 of the vertical headwall and the length of the gully bed are 5.0 m long, 0.9 m, and 1.0 m, respectively
 159 (Fig. 1a). The plot boundary was constructed in strict accordance with designed plot dimension using
 160 cement and bricks (Fig. 1b). After the construction of plot boundary, the soil was sieved through a 2
 161 cm sieve to remove roots and debris and ensure uniform soil underlying condition. The sieved soil was
 162 filled into the plot every 10-cm thick layer according to the investigated soil bulk density of gully
 163 heads. The soil surface of each layer was harrowed to increase the cohesion between two soil layers
 164 (Guo et al., 2019). In general, the filling upstream area length was 5.5 m that was larger than the precise
 165 upstream area length (5.0 m). After establishment of gully head plots, the five plots were carefully
 166 managed about four months (August 2018) to allow the soil to return to its nearly natural state. During
 167 the four-month conservation process, the naturally growing weeds were weeded out in time. Moreover,
 168 a flow-steady tank of 0.6 m, 1.5 m and 0.5 m in length, width and height was installed at the top of
 169 upstream area, and a circular sampling pool of 0.6 m in diameter was set at the bottom of the gully bed
 170 to collect runoff and sediment (Fig. 1a). According to the pre-experimental results, the length of
 171 upstream area can meet the needs of headcut migration under designed flow discharge ($3.0 - 7.2 \text{ m}^3 \text{ h}^{-1}$)
 172 and gully head height (0.9 m), and the length of gully bed also can satisfy the development of plunge
 173 pool by jet flow and stabilize the flow of gully bed.



174
 175 **Figure 1.** Sketch (a) and photo (b) of experimental plot

176 **2.2.2 Inflow discharge design**

177 The concentrated runoff generated from upstream area is the main force driving gully headcut

178 erosion. Jiao et al (1999) concluded that the more serious soil erosion is generally caused by “A” type
 179 rainstorm with the rainfall duration of 25 to 178 mins than other types of rainstorms in the Loess
 180 Plateau. Thus, an extreme case of rainfall duration (180 min) was considered in this study, and the
 181 recurrence period of “A” type rainstorm was designed as 30 years. Previous studies indicated that the
 182 rainstorm distribution on the Loess Plateau showed a non-significant change in past decades (Li et al.,
 183 2010; Sun et al., 2016; Wen et al., 2017). Zhang et al. (1983) proposed a statistical equation (Eq. (1))
 184 for calculating the average rainfall intensity by analyzing 1710 typical rainstorm events in the Loess
 185 Plateau. Then, the inflow discharge was calculated by Eq. (2) that involves the runoff coefficient, storm
 186 intensity and drainage area upstream gully head and ranged from 3.12 to 9.68 m³ h⁻¹. Before the study,
 187 we first conducted some preliminary experiments under some flow discharges, and meanwhile
 188 considering the pre-experiment effect, finally, we selected the five inflow discharge levels (3.0, 3.6,
 189 4.8, 6.0, and 7.2 m³ h⁻¹).

$$190 \quad RI = \frac{5.09N^{0.379}}{(t+1.4)^{0.74}} \quad (1)$$

191 where RI is the average rainfall intensity during t minutes, mm min⁻¹; N is the recurrence period
 192 of rainstorm, yr; and t is the rainfall duration, min.

$$193 \quad q = \frac{60\alpha \cdot A \cdot RI \cdot w}{W} \quad (2)$$

194 where A is the upstream area (km²) and has a wide range of 0.15 - 8.7 km² according to an early
 195 investigation of research team (Che, 2012); W is the width of the upstream area, km; w is the plot width,
 196 m; and α is the runoff coefficient of bare land and is identified as 0.167 by analyzing the runoff and
 197 rainfall data of standard runoff plots (Li et al., 2006).

198 **2.3 Experimental procedure**

199 The scouring experiment was conducted in August 2018. Before formal experiment, the upstream
 200 area length was firstly adjusted to designed length of 5.0 m (Fig. 2a). Then, a self-made tent (length ×
 201 width × height: 6.0 m × 3.0 m × 3.5 m) with waterproof canvas enclosed the plot to resist the effects
 202 of natural rainfall and sunshine on experimental progress and photo shooting for 3D reconstruction
 203 (Fig. 1b). In addition, the experimental process was recorded by two Logitech 930e video cameras
 204 with a resolution of 2.0 megapixels. The camera 1 was installed 2.5 m in front of plot headwall (Fig.
 205 1a), and the camera 2 was installed 3.0 m above the plot center (Fig. 1a).

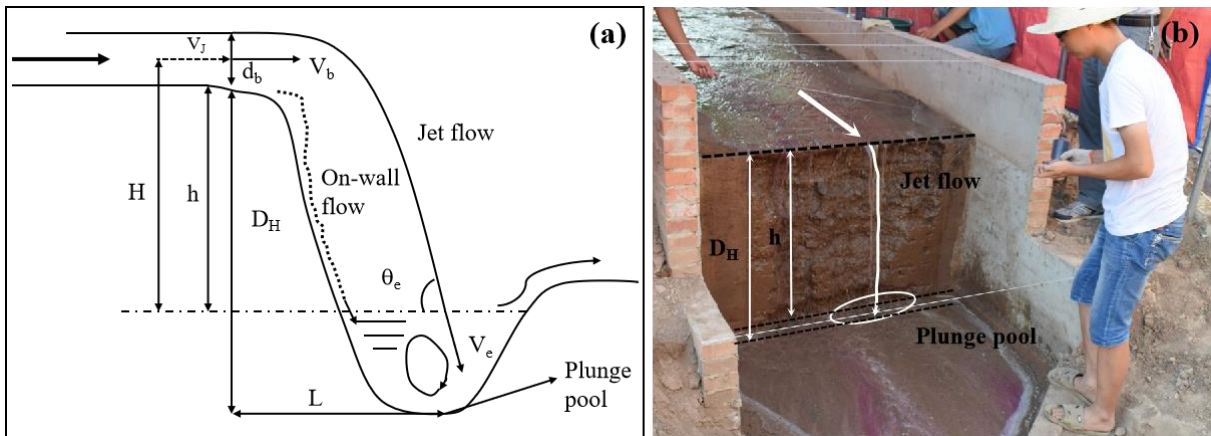
206 Before the experiment, watering can be used to spray each experimental plot until surface runoff
207 was generated, and then the plot was placed for 24 hours to ensure adequate water infiltration, which
208 can assure that the soil moisture of the five plots was approximately the same. The inlet pipeline was
209 placed in steady flow tank when the inflow discharge was adjusted to designed value. A water
210 thermometer was placed into the steady flow tank to monitor the change in water temperature during
211 experiments. The runoff and sediment samples at the plot outlet were collected at 2-min intervals to
212 represent the temporal change in runoff and sediment of “UA-GH-GB” system, and the sampling time
213 was recorded using a stopwatch (Fig. 2b). The runoff and sediment samples were oven-dried at 105 °C
214 for 24 h and weighed to calculate the soil loss rate of “UA-GH-GB” system. Besides, the timing of the
215 collapse event was recorded during headcut erosion. The upstream area was divided into 4 runoff
216 observation sections, and the runoff width (w), depth (d) and velocity (V) of each section were
217 measured by a calibrated scale of 1 mm accuracy and color tracer method (Fig. 2b, 2c). The runoff
218 velocity (V_r) before runoff arrived at the brink of headcut was measured 5 – 8 times by the flow velocity
219 measuring instrument (LS300-A). The instrument was firstly placed perpendicular to the flow section
220 but does not touch the underlying surface. When the flow passes through the turbine, the flow velocity
221 can be measured by the rotating velocity of the turbine with the accuracy of 0.01 m s⁻¹ and measuring
222 error of < 1.5%, and the runoff width at the headcut brinkpoint was measured (Fig. 2d). The runoff
223 width and velocity of gully bed were also measured using the same method with upstream area (Fig.
224 2e). Above mentioned measurements of runoff characteristics and sediment samples were finished in
225 2-min intervals. The whole experimental process was recorded by two video cameras and imported
226 into computers (Fig. 2f). In addition to above runoff parameters, the runoff depth (d_b) at the brink of
227 headcut, the plunge pool depth (D_H) and the vertical distance (h) from brink-point of headcut to water
228 surface of plunge pool were also measured 3 - 5 times by a steel ruler with 1 mm accuracy within each
229 2-min intervals (Fig. 3).

230



231
232
233
234
235
236

Figure 2. Plot construction (a), runoff width measurement of loess-tableland and runoff and sediment sampling of outlet (b), runoff velocity measurement of loess-tableland (c), jet velocity measurement of gully head (d), runoff velocity and width measurement of gully bed (e), and experimental process recoding (f)



237
238

Figure 3. Sketch of jet flow at gully headcut (a) and plunge pool at gully bed (b)

239

240

241

242

243

244

245

246

To obtain the dynamic change in morphology of erosional landform during gully headcut erosion, the experimental duration (180 min) was divided into six stages (30 - 60 - 90 - 120 - 150 - 180 min). Photo-based three-dimensional (3D) reconstruction method was employed to obtain the digital elevation model (DEM) data of each plot prior to experiment and after each 30-min test. A total of 14 target points were placed around the plot for identifying the 3D coordinate before the photos were taken. The eroded photographic was recorded by a Nikon D5300 camera with the focal length of 50 mm. The following aspects were required during photos shooting: (1) obvious water on soil surface and direct sunshine should be avoided, (2) a minimum overlap of 60% between subsequent

247 photographs was required, and (3) some complex eroded photographic should be taken in detail. In
 248 this study, the upper left corner of the plot was set as the original coordinates (0, 0, 0), and the direction
 249 of three-dimensional coordinate was determined as shown in Fig. 3d. These collected photos were
 250 imported in Agisoft PhotoScan software (Agisoft LLC, Russia, professional version 1.1.6), and then
 251 these control points and their coordinates would be identified and entered into the software. The root
 252 mean square errors for the altitudes (Z axis) of the target points are 0.0037, 0.0045, 0.0024, 0.0052 and
 253 0.0030 m on average, respectively, for the experiments of five inflow discharges, which can satisfy the
 254 study requirement (millimeter level). The DEM could be exported and was used to extract the
 255 morphological parameters and soil loss volume of three landform units at six stages (Frankl et al.,
 256 2015).

257 **2.4 Parameter calculation, data analysis and figure plotting**

258 **2.4.1 Hydraulic parameters of upstream area and gully bed**

259 Five parameters including runoff velocity (V , m s^{-1}), Reynold number (Re), Froude number (Fr),
 260 shear stress (τ , Pa) and stream power (ω , W m^{-2}) were used to characterize the changes in hydraulic
 261 properties at upstream area and gully bed positions. The several parameters except for V are calculated
 262 as follows.

$$263 \quad Re = \frac{V \cdot R}{\nu} \quad (1)$$

$$264 \quad Fr = \frac{V}{\sqrt{g \cdot R}} \quad (2)$$

$$265 \quad R = \frac{w \cdot d}{w + 2d}, \nu = \frac{1.775 \times 10^{-6}}{1 + 0.0337T + 0.000221T^2} \quad (3)$$

$$266 \quad \tau = \rho_w \cdot g \cdot R \cdot J \quad (4)$$

$$267 \quad \omega = \tau \cdot V \quad (5)$$

268 where R (m) and ν ($\text{m}^2 \text{s}^{-1}$) are the hydraulic radius and the water kinematic viscosity coefficient,
 269 respectively; w (m), d (m) and T ($^{\circ}\text{C}$) are the runoff width, depth and water temperature, respectively;
 270 ρ_w (kg m^{-3}) is the water density and J (m m^{-1}) is the hydraulic gradient.

271 **2.4.2 Jet properties of gully head**

272 Based on the measured runoff velocity (V_J , m s^{-1}) before runoff arrived at the headcut brinkpoint,
 273 the runoff depth (d_b , m) at the headcut brinkpoint, the plunge pool depth (D_H , m) and the vertical

274 distance (h , m) (Fig. 3a), the three parameters including the runoff velocity at the headcut brinkpoint
 275 (V_b), jet-flow velocity entry to plunge pool (V_e) and jet-flow shear stress (τ_j) were calculated to clarify
 276 the change of jet properties (Rouse, 1950; Hager, 1983; Stein et al., 1993; Flores-Cervantes et al., 2006;
 277 Zhang et al., 2016). The three parameters were calculated as follows.

$$278 \quad V_b = \begin{cases} \frac{\sqrt[3]{q \cdot g}}{0.715}, Fr < 1 \\ V_J \cdot \frac{Fr^2 + 0.4}{Fr^2}, Fr > 1 \end{cases} \quad (5)$$

$$279 \quad Fr = \frac{V_J}{\sqrt{g \cdot d_b}} \quad (6)$$

$$280 \quad V_e = \frac{V_b}{\cos \theta_e}, \theta_e = \arctan \left(\frac{\sqrt{2g \cdot D_H}}{V_b} \right) \quad (7)$$

$$281 \quad \tau_j = 0.025 \left(\frac{v}{q} \right)^{0.2} \cdot \rho_w \cdot [2g \cdot (h + d_b/2) + V_b^2] \quad (8)$$

282 2.4.3 Energy consumption of upstream area, gully head and gully bed

283 In this study, energy consumption of three landform units (UA, GH, GB) were calculated
 284 according to the measured runoff characteristic parameters. The bottom of GB was treated as the zero
 285 potential surface to quantify the energy consumption. Therefore, the total runoff energy (E_T , J s⁻¹), the
 286 runoff energy at the brink of headcut (E_L , J s⁻¹), the runoff energy when runoff leaves the plunge pool
 287 (E_H , J s⁻¹), and the runoff energy at the bottom of gully bed (E_B , J s⁻¹) were calculated as following.
 288 The calculation was consistent with the theory of minimum rate of energy dissipation expressed by
 289 Yang (1971a, 1971b).

$$290 \quad E_T = \rho_w g q [(L_l + L_g) \tan \theta + H_h] \quad (9)$$

$$291 \quad E_L = \rho_w g q [(L_m + L_g) \tan \theta + H_h] + \frac{1}{2} \rho_w q V_J^2 \quad (10)$$

$$292 \quad E_H = \rho_w g q \left(L_m + L_g - V_b \sqrt{\frac{2h}{g}} \right) \tan \theta + \frac{1}{2} \rho_w q V_P^2 \quad (11)$$

$$293 \quad E_B = \frac{1}{2} \rho_w q V_B^2 \quad (12)$$

294 where the L_l (m) and L_g (m) are the projection length of UA and GB, respectively, during gully
 295 head migration; L_m (m) is the gully head retreat distance; H_h (m) is the initial gully headcut height. V_P
 296 (m s⁻¹) and V_B (m s⁻¹) are the runoff velocity runoff leaving the plunge pool and GB, respectively.

297 Therefore, the total runoff energy consumption (ΔE_T , J s⁻¹), the runoff energy consumption of UA
 298 (ΔE_L , J s⁻¹), the runoff energy consumption of GH (ΔE_H , J s⁻¹) and the runoff energy consumption of

299 GB ($\Delta E_B, \text{J s}^{-1}$) could be calculated as follows.

300
$$\Delta E_T = E_T - E_B \quad (13)$$

301
$$\Delta E_L = E_T - E_L \quad (14)$$

302
$$\Delta E_H = E_L - E_H \quad (15)$$

303
$$\Delta E_B = E_H - E_B \quad (16)$$

304 **2.4.4 Statistical analysis**

305 The curve regression analysis method was employed to determine the quantitative relations
306 between hydraulic characteristics, jet properties, runoff energy consumption and soil erosion rate and
307 inflow discharge. The fitted equations between soil loss rate of three landform units and hydraulic
308 characteristics, jet properties, and energy consumption were also quantified by the curve regression.
309 The soil erosion volume of upstream area, gully head and gully bed were derived from the DEM of
310 different stages through the ArcGIS 10.0 software. The data analyse was executed by using SPSS
311 software (version 6.0) and figure plotting was carried out with Origin 8.5 and PowerPoint 2016
312 software.

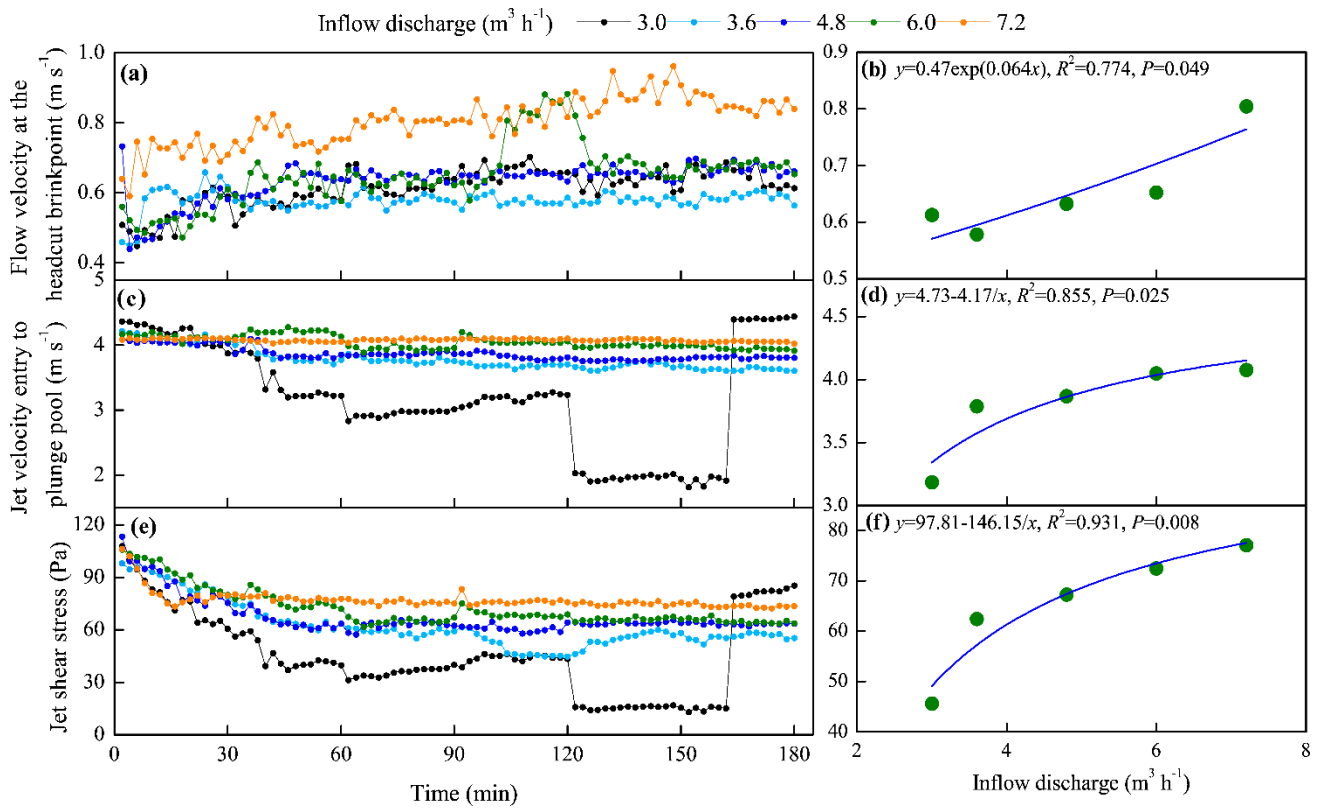
313 **3 Results**

314 **3.1 Spatial-temporal changes in jet properties and runoff hydraulic**

315 **3.1.1 Jet properties of gully head**

316 Fig. 4 shows the temporal change in the three jet property parameters of gully head (GH) under
317 different inflow discharge conditions. Overall, the flow velocity at the headcut brinkpoint (V_b)
318 increased obviously in the first 30 min and then showed a gradually stable tendency with some degree
319 of fluctuation (Fig. 4a), and the fluctuation degree was enhanced by the increased inflow discharge.
320 For example, the V_b increased sharply from 0.66 to 0.88 m s^{-1} during 100 - 124 min under 6.0 $\text{m}^3 \text{h}^{-1}$
321 inflow discharge due to the headwall failure near headcut enhancing the runoff turbulence. Regression
322 analysis revealed the significant power relationships ($V_b = a \cdot t^b$, $R^2 = 0.139 - 0.704$, $P < 0.01$) between
323 V_b and time (t) (Table 1). Furthermore, except for 3.6 $\text{m}^3 \text{h}^{-1}$ condition, the a -value increased with the
324 inflow discharge increased, but the b -value showed a weak variation (0.08 - 0.10), indicating that the
325 flow drainage from gully head can improve initial V_b but not change its change trend over time. The
326 mean V_b exhibited a significantly exponential relationship with inflow discharge (Fig. 4b, $P < 0.05$).

327 Contrary to the V_b , the jet velocity entry to plunge pool (V_e) and the jet shear stress (τ_j) experienced a
 328 gradually decreased trend with time (Fig. 4c, 4e). Notably, the V_e and τ_j suddenly decreased at 120th
 329 min and lasted nearly 40 minutes under $3.0 \text{ m}^3 \text{ h}^{-1}$ inflow discharge, which was mainly attributed to
 330 the developed second headcut shortening the jet-flow height. The temporal change of V_e could be
 331 described by logarithmic functions under $3.0 - 4.8 \text{ m}^3 \text{ h}^{-1}$ inflow discharges, and expressed by linear
 332 functions under the other inflow discharges, whereas the decrease of the τ_j with time could be presented
 333 by logarithmic functions under all inflow discharge conditions (Table 1). Furthermore, both of mean
 334 V_e and τ_j could be expressed by a positive “S” function of inflow discharge (Fig. 4d, 4f).



335

336

337

Figure 4. Temporal changes in jet properties of headcut and their relationships with inflow discharge

Table 1. The relationships between jet properties of gully headcut and time

Inflow discharge ($\text{m}^3 \text{ h}^{-1}$)	$V_b \sim t$	$V_e \sim t$	$\tau_j \sim t$
3.0	$V_b = 0.42 t^{0.09}, R^2=0.691$	$V_e = 5.28-0.49 \lg(t), R^2 = 0.290$	$\tau_j = 110.86-15.44 \lg(t), R^2 = 0.344$
3.6	$V_b = 0.53 t^{0.02}, R^2 = 0.139$	$V_e = 4.52-0.17 \lg(t), R^2 = 0.859$	$\tau_j = 117.93-13.14 \lg(t), R^2 = 0.823$
4.8	$V_b = 0.46 t^{0.08}, R^2 = 0.544$	$V_e = 4.25-0.09 \lg(t), R^2 = 0.718$	$\tau_j = 109.22-9.93 \lg(t), R^2=0.770$
6.0	$V_b = 0.52 t^{0.10}, R^2 = 0.509$	$V_e = 4.17-1.33 \times 10^{-3} t, R^2 = 0.478$	$\tau_j = 118.73-10.96 \lg(t), R^2 = 0.876$
7.2	$V_b = 0.57 t^{0.08}, R^2 = 0.704$	$V_e = 4.09-1.38 \times 10^{-4} t, R^2 = 0.111$	$\tau_j = 95.68-4.42 \lg(t), R^2 = 0.619$

338

339

Note: V_b , V_e and τ_j are runoff velocity at the headcut brinkpoint, runoff velocity entry to plunge pool and the jet shear stress, respectively. The sample number is 90 for the fitted equations, and all fitted equations are at 0.01 significant

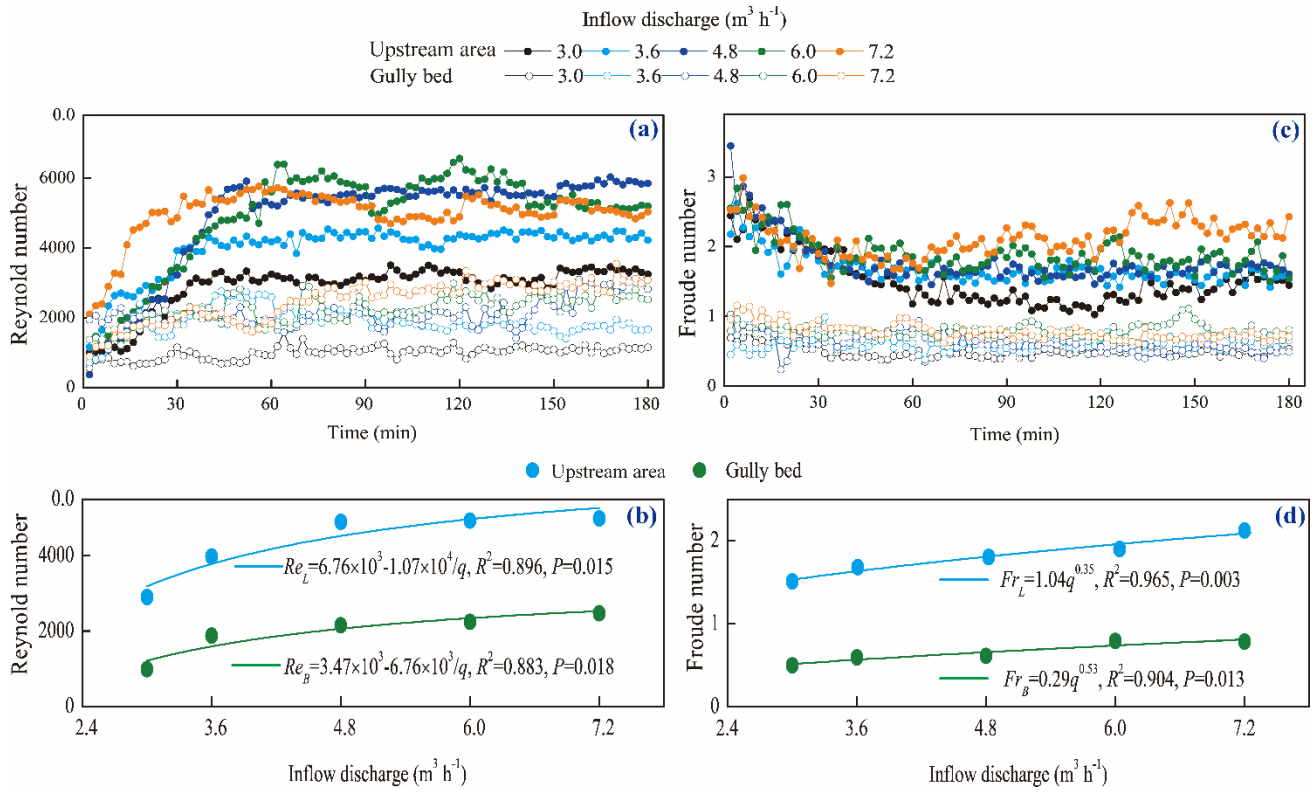
340 level.

341 **3.1.2 Runoff regime of upstream area and gully bed**

342 The temporal changes in runoff Reynold number (Re) and Froude number (Fr) of upstream area
343 (UA) and gully bed (GB) and their relationships with inflow discharge are provided in Fig. 5. The Re
344 of UA and GB showed a similar trend over time, that is, the Re firstly increased in the first 40 min and
345 then gradually stabilized (Fig. 5a). In addition, the Re of UA was larger than that of GB at any time
346 under same inflow discharge, indicating that the runoff turbulence became weaker after the runoff of
347 UA passed the gully head. The temporal variation in Re of UA could be described by logarithmic and
348 power functions, but, for the GB, the relationship was mainly dominated by power function (Table 2).
349 On average, the Re of GB was 50.5% - 65.9% less than that of UA, and the Re of UA and GB both
350 increased with the increase of inflow discharge as a power function (Fig. 5b). However, as illustrated
351 in Fig. 5c, the Fr experienced a completely opposite trend to Re . The Fr of UA decreased in the first
352 60 min and then gradually stabilized, but the Fr of GB experienced a relatively weak-fluctuating
353 variation over time. For the most of cases, the change in Fr of UA and GB over time could be expressed
354 by logarithmic functions (Table 2). On average, the Fr of UA was 2.39 - 3.04 times that of GB for
355 same inflow discharge, and the positive power function could describe the relationship between Fr and
356 inflow discharge (Fig. 5d).

357 Furthermore, the knowledge of open channel hydraulics is adopted to investigate the difference
358 in runoff regime between UA and GB. The specific definition is: the flow belongs to laminar when Re
359 is less than 500, the flow is turbulent when Re is larger than 2000, and the flow indicates transitional
360 when Re ranges from 500 to 2000; and $Fr = 1$ is the critical value for to distinguish the subcritical and
361 supercritical flow. The six flow regime zones were divided by three boundary lines ($Re = 500$, $Re =$
362 2000 , and $Fr = 1$) according to the logarithmic relationship between the flow velocity and hydraulic
363 radius (Fig. 6) (Xu et al., 2017b; Guo et al., 2020b). As shown, the runoff regimes of UA and GB were
364 located in five entirely different zones. The flow of UA was in the supercritical-transition flow regime
365 in the first 26 min and then gradually transformed to supercritical-turbulent flow regime under 3.0 -
366 $6.0 \text{ m}^3 \text{ h}^{-1}$ inflow discharge, but the flow was always in the supercritical-turbulent regime zone under
367 $7.2 \text{ m}^3 \text{ h}^{-1}$ inflow discharge. Moreover, the higher inflow discharge would enhance the flow turbulent

368 degree. The flow of GB belonged to subcritical-laminar flow category in the initial 6 min, and then
 369 transformed to subcritical-transition and subcritical-turbulent flow regime when inflow discharge was
 370 3.0 and 3.6 m³ h⁻¹. The flow was in the subcritical-turbulent flow regime in most of experimental
 371 duration when the inflow discharge was 4.8 - 7.2 m³ h⁻¹. The difference in flow regime between UA
 372 and GB also indicated that the presence of gully head can greatly reduce flow turbulence.



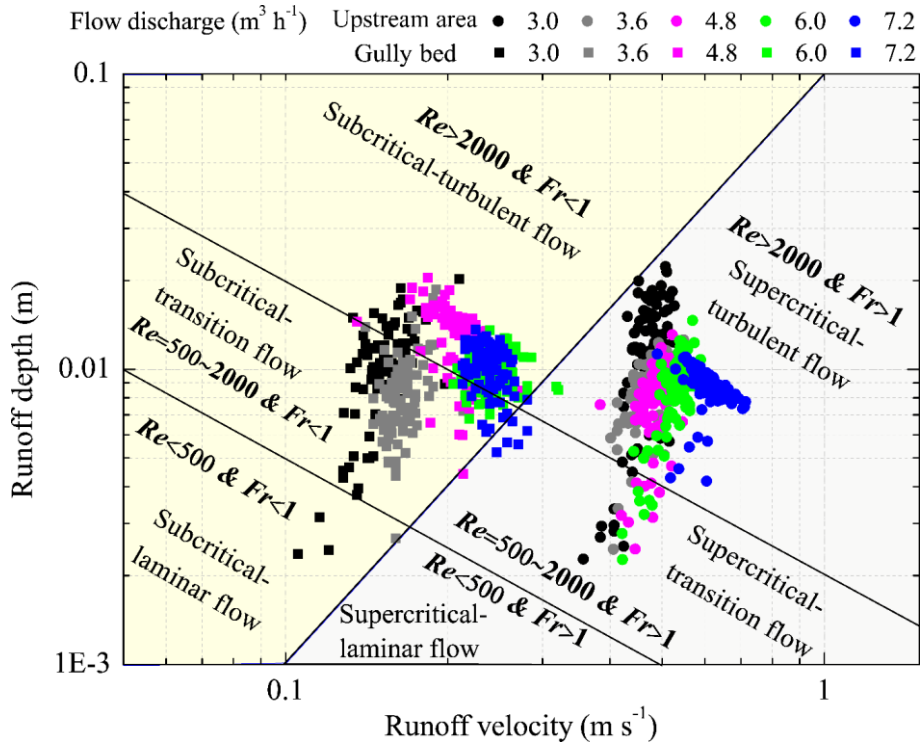
373
 374 **Figure 5.** Temporal changes in runoff regime of upstream area and gully bed and their relationships with inflow
 375 discharge
 376

Table 2. Relationships between runoff hydraulic parameters and time

Variable	Landfor m unit	Inflow discharge (m ³ h ⁻¹)				
		3.0	3.6	4.8	6.0	7.2
Reynold number	UA	$Re = 618.69 \lg(t) + 286.69, R^2 = 0.761$	$Re = 705.93 \lg(t) + 1006, R^2 = 0.815$	$Re = 1433 \lg(t) - 1159, R^2 = 0.849$	$Re = 946.64 t^{0.38}, R^2 = 0.794$	$Re = 2760 t^{0.14}, R^2 = 0.486$
	GB	$Re = 514.36 t^{0.15}, R^2 = 0.504$	—	$Re = 4.31 t + 1760, R^2 = 0.334$	$Re = 1.12 \times 10^3 t^{0.16}, R^2 = 0.566$	$Re = 744.99 t^{0.28}, R^2 = 0.872$
Froude number	UA	$Fr = 2.89 - 0.33 \lg(t), R^2 = 0.651$	$Fr = 2.46 - 0.19 \lg(t), R^2 = 0.651$	$Fr = 3.27 - 0.35 \lg(t), R^2 = 0.656$	$Fr = 2.76 - 0.20 \lg(t), R^2 = 0.515$	—
	GB	$Fr = 0.72 - 0.05 \lg(t), R^2 = 0.326$	—	$Fr = 1.0 - 0.09 \lg(t), R^2 = 0.359$	—	$Fr = 1.21 - 0.10 \lg(t), R^2 = 0.634$
Shear stress	UA	$\tau = 0.66 \lg(t) + 0.55, R^2 = 0.737$	$\tau = 1.18 \lg(t) + 0.78, R^2 = 0.813$	$\tau = 1.32 \lg(t) - 0.62, R^2 = 0.817$	$\tau = 1.50 \lg(t) - 0.63, R^2 = 0.663$	$\tau = 1.11 \lg(t) + 0.99, R^2 = 0.819$
	GB	$\tau = 2.44 t^{0.08}, R^2 = 0.205$	$\tau = 3.88 t^{0.05}, R^2 = 0.106$	$\tau = 2.27 t^{0.19}, R^2 = 0.664$	$\tau = 3.64 t^{0.12}, R^2 = 0.212$	$\tau = 1.99 t^{0.27}, R^2 = 0.686$

Stream	UA	$\omega = 0.34 \lg(t) + 0.16, R^2 = 0.761$	$\omega = 0.38 \lg(t) + 0.55, R^2 = 0.815$	$\omega = 0.78 \lg(t) - 0.63, R^2 = 0.849$	$\omega = 0.69 \lg(t) - 0.23, R^2 = 0.737$	$\omega = 0.27 \lg(t) + 1.56, R^2 = 0.436$
power	GB	$\omega = 0.28 t^{0.15}, R^2 = 0.504$	$\omega = 0.69 t^{0.09}, R^2 = 0.123$	$\omega = 0.50 t^{0.19}, R^2 = 0.540$	$\omega = 0.83 t^{0.09}, R^2 = 0.338$	$\omega = 0.51 t^{0.23}, R^2 = 0.806$

377 Note: UA and GB refer to upstream area and gully bed. Re , Fr , τ and ω are Reynold number, Froude number, shear
378 stress, stream power, respectively. The sample number is 90 for the fitted equations, and the fitted equations are at
379 0.01 significant level.

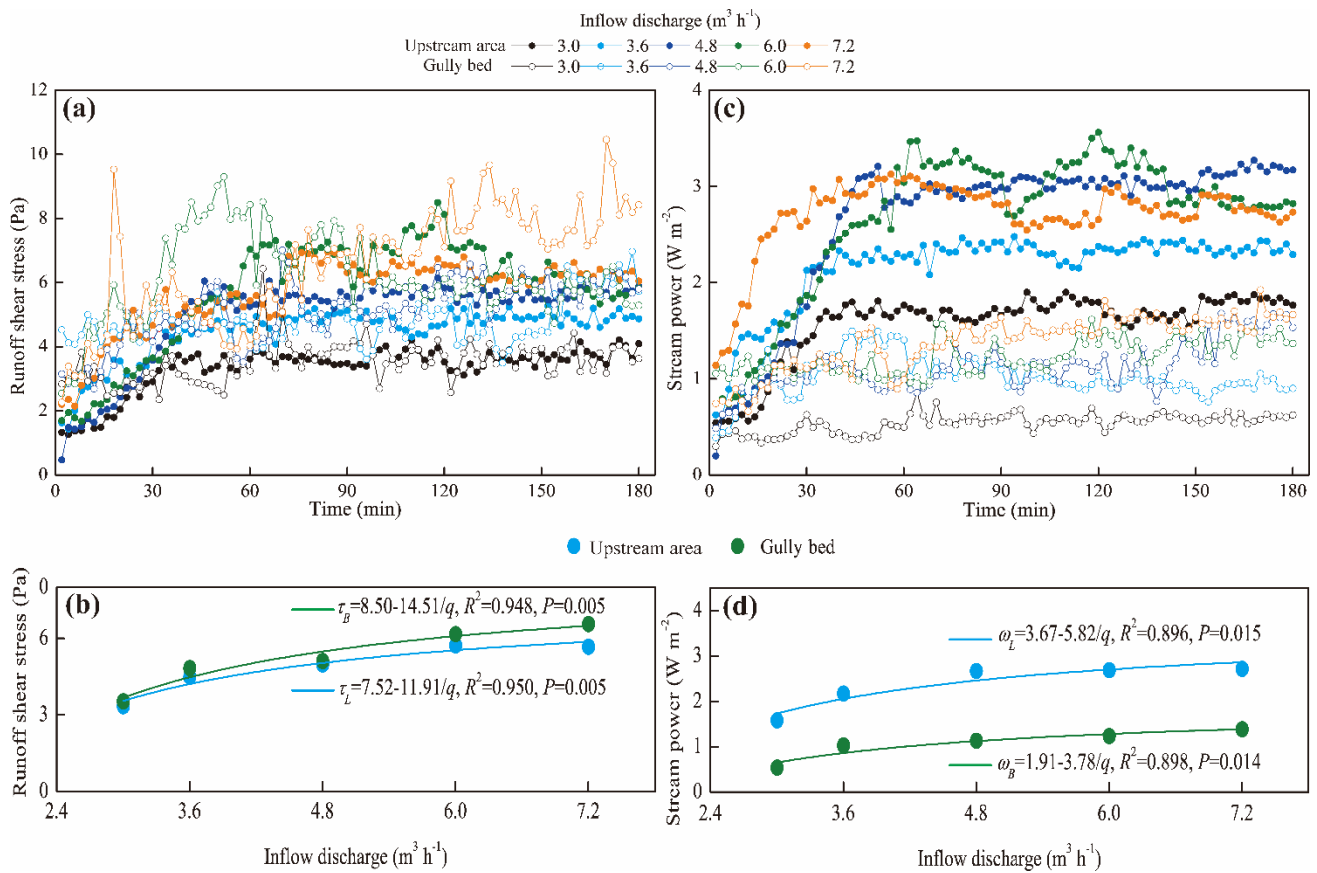


380
381 **Figure 6.** Runoff regime zones of upstream area and gully bed under different inflow discharge conditions.

382 3.1.3 Runoff shear stress and stream power of upstream area and gully bed

383 Fig.7 shows the temporal changes in runoff shear stress (τ) and stream power (ω) of upstream
384 area (UA) and gully bed (GB) and their relationships with inflow discharge. Overall, the τ of UA and
385 GB exhibited a gradually increased trend in the first 60 min, and whereafter, a relative steady state was
386 obtained, but the larger inflow discharge perturbed the steady situation (Fig. 7a). Furthermore, the
387 temporal change in τ of UA could be expressed by logarithmic functions, but the τ of GB showed a
388 significant power function with experimental time (Table 2). On average, the τ of GB was 2.8% - 15.7%
389 larger than the UA. The averaged τ of UA and GB increased with inflow discharge as a power function
390 ($\tau = a - b/q$), and the GB had a faster increased-speed (b -value) than UA (Fig. 7b), signifying that the
391 difference in τ between UA and GB would be widened with the inflow discharge increased. Similarly,
392 the ω of UA and GB also exhibited a trend of gradual increase and stabilization (Fig. 7c). Different

393 from the temporal change in τ , the ω of GB was always less than that of UA at any time for five inflow
 394 discharges. Likewise, the variation in ω of UA and GB over time exhibited a significant logarithmic
 395 and power function, respectively. On average, the ω of GB was 49.2% - 65.9% less than UA, and the
 396 positive increase in ω of UA and GB with inflow discharge could be expressed by a power function
 397 (Fig. 7d).



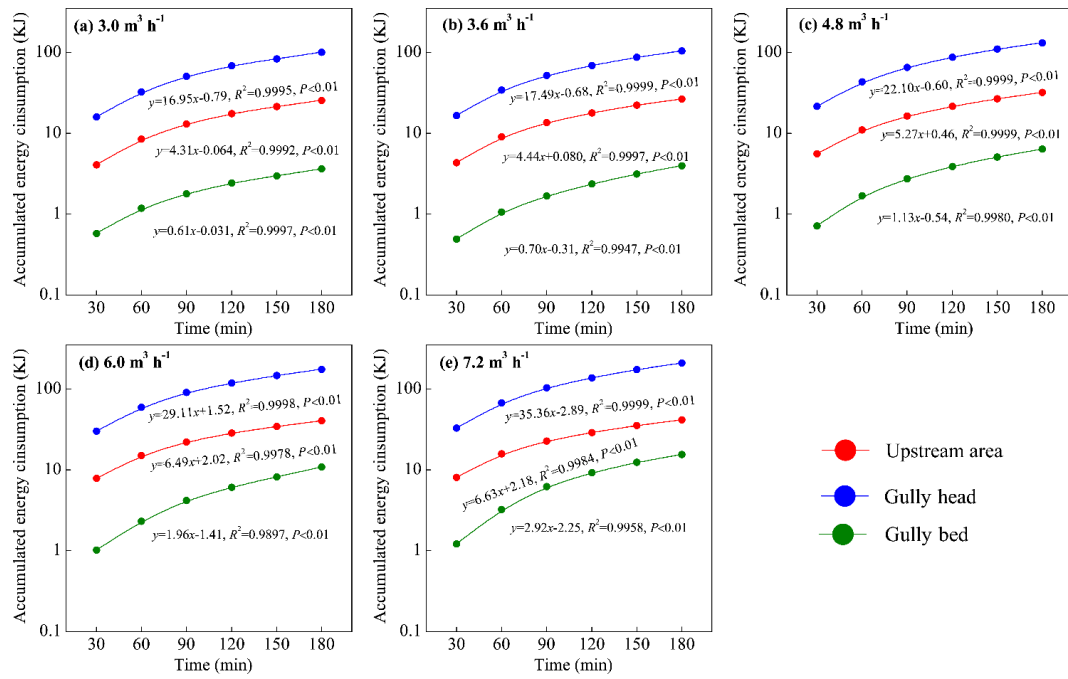
398
 399 **Figure 7.** Temporal changes in runoff shear stress and stream power of upstream area and gully bed and their
 400 relationships with inflow discharge

401 3.2 Spatial-temporal change of energy consumption

402 Fig. 8 illustrates the temporal change in accumulated energy consumption of upstream area (UA),
 403 gully head (GH) and gully bed (GB). The accumulated energy consumption of the three landform units
 404 continued to linearly increase with time ($R^2 = 0.990 - 0.999$, $P < 0.01$), of which the accumulated energy
 405 consumption in GH was always the highest at any time, followed by UA and GB under five inflow
 406 discharges. Moreover, the energy consumption rate (the slope-value of fitted equation) in the three
 407 landform units is basically constant, indicating the spatial-temporal change in energy consumption
 408 maintained a relatively steady state during gully headcut erosion. Moreover, the energy consumption

409 rate of GH was the highest, followed by UA and GB, and the energy consumption rate in the three
410 landform units also increased with the increase of inflow discharge.

411 The variations of total energy consumption of UA, GH and GB and their proportions with inflow
412 discharge are shown in Fig. 9. As illustrated in Fig. 9a, both of the total energy consumption of the
413 “UA-GH-GB” system and the three landform units increased with the increase of inflow discharge.
414 When inflow discharge increased from 3.0 to 7.2 m³ h⁻¹, the total energy consumption of the system,
415 UA, GH and GB increased by 3.6% - 105.3%, 3.4% - 62.0%, 3.5% - 108.2% and 9.0% - 327.5%,
416 respectively. Regression analysis revealed that the energy consumption of the system and the three
417 landform units increased with inflow discharge as an exponential function ($y = a \cdot \exp(b \cdot x)$, $a = 1.14 -$
418 55.41 , $b = 0.13 - 0.36$, $R^2 = 0.954 - 0.992$, $P < 0.05$). Furthermore, in view of the proportion of energy
419 consumption, the energy consumption of UA accounted for 15.6% - 19.8% of total energy consumption,
420 and linearly decreased with inflow discharge increased ($R^2 = 0.933$, $P < 0.05$), whereas the proportion
421 in GB (2.8% - 5.8%) linearly increased with inflow discharge increased ($R^2 = 0.983$, $P < 0.05$). However,
422 the proportion of energy consumption (77.3% - 78.6%) in GH showed a weak change with inflow
423 discharge (Fig. 9b), signifying that the most of runoff energy (77.5% on average) was consumed in the
424 gully head position during headcut migration. Furthermore, we found that the total energy consumption
425 (129.89 - 266.60 KJ) under different flow discharge conditions accounted for the 91.12% - 99.90% of
426 total flow energy (Fig. 9c, 9d), which also indicated that only 0.10% - 8.88% of total flow energy
427 remained at the outlet of the “UA-GH-GB” system. These results fully implied that the most of flow
428 energy (>91.12%) upstream from gully heads would be consumed during gully erosion, of which the
429 gully headcut erosion (including plunge pool erosion) is the main process consuming flow energy.

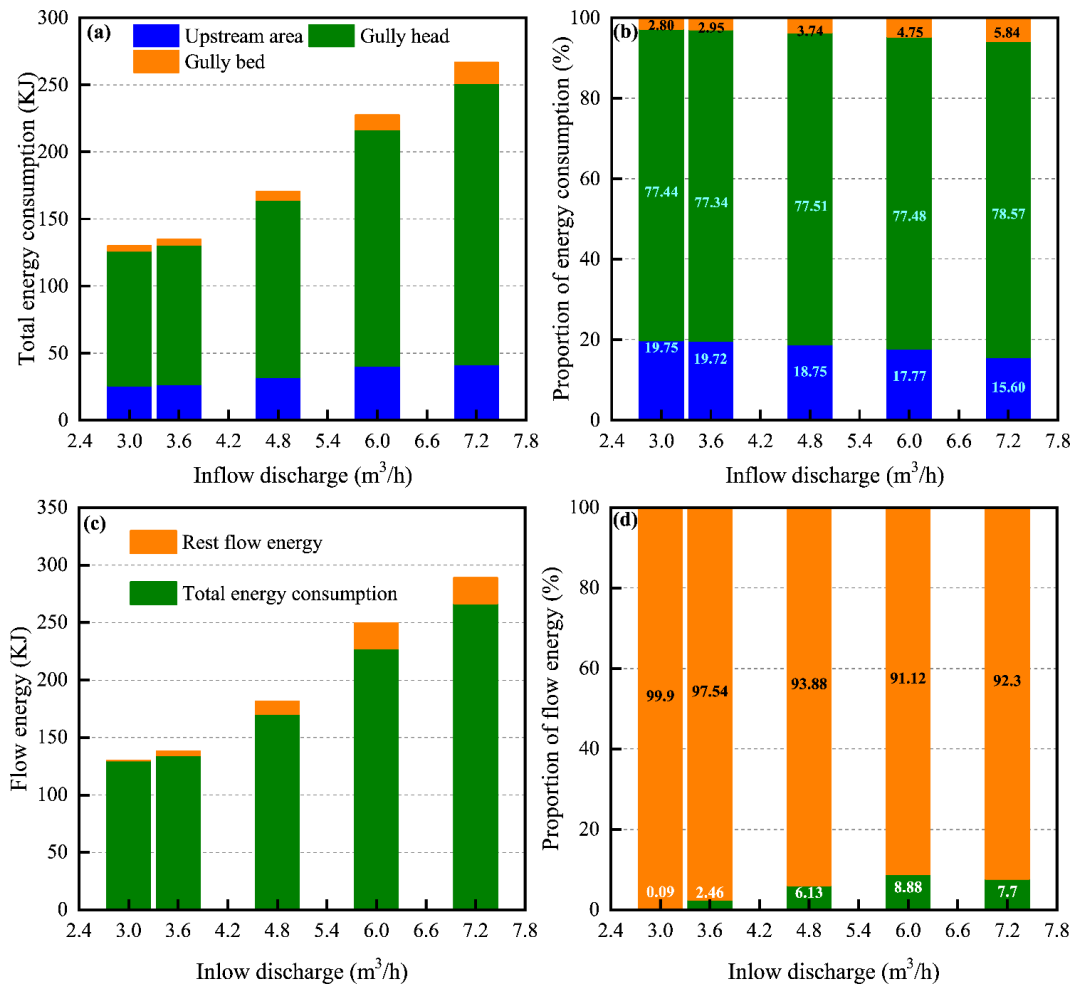


430

431

432

Figure 8. Temporal changes in runoff energy consumption of upstream area, gully head and gully bed under different inflow discharge conditions



433

434

Figure 9. Total energy consumption (a) and their proportions (b) of upstream area, gully head and gully bed, and

435 the total energy consumption and rest flow energy (c) and their proportions (d) with under different inflow
436 discharge conditions

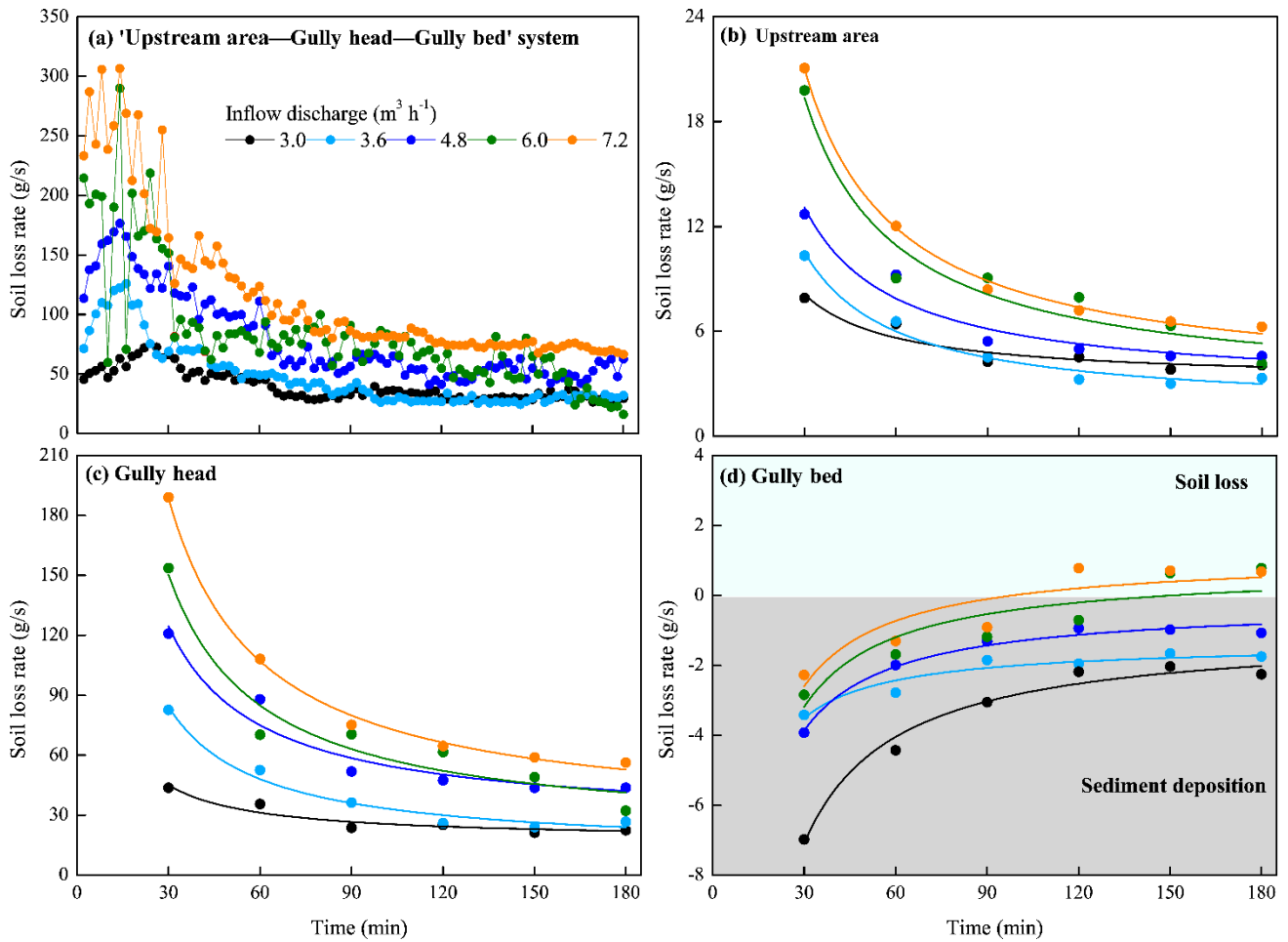
437 **3.3 Spatial-temporal change of soil loss**

438 **3.3.1 Soil loss process**

439 Fig. 10a shows that the soil loss rate of the “upstream area (UA)-gully head (GH)-gully bed (GB)”
440 system rose to a peak in first 20 min, then gradually descend and levelled off. Especially for the 6.0
441 and 7.2 m³ h⁻¹, the soil loss rate showed a severe fluctuation trend in the first 30 min. The peak soil
442 loss rate increased from 75.4 to 306.9 g s⁻¹ with increasing inflow discharge. The soil loss of UA and
443 GH experienced a similar change process. The soil loss rate was the highest in the early stage of the
444 experiment, and gradually decreased with time, and became stable after 120 min (Fig. 10b, 10c).
445 Furthermore, the temporal variation in soil loss of UA and GH could be well expressed by logarithmic
446 function ($S_L = a - b \cdot \ln(t)$, $P < 0.05$, Table 3), and the a -value (representing initial soil loss rate) and b -
447 value (reflecting the reduction rate of soil loss rate with time) increased with increasing inflow
448 discharge, indicating that larger inflow discharge can improve initial soil loss of UA and GH and also
449 expedite the decrease of soil loss rate.

450 However, the GB presented a completely different soil loss process from UA and GH (Fig. 10d).
451 The GB was always characterized by sediment deposition during the whole experiment for the 3.0 -
452 4.8 m³ h⁻¹ inflow discharges. The sediment deposition rate gradually decreased with time and presented
453 a significant “S” function over time ($S_B = a/t - b$, $R^2 = 0.918 - 0.982$, $P < 0.01$, Table 3). When the inflow
454 discharge was larger than 4.8 m³ h⁻¹, the sediment generated from UA and GH was deposited firstly in
455 the GB and then gradually transported, and the temporal change of deposited sediment on GB accorded
456 with logarithmic functions ($R^2 = 0.936$ and 0.906 , $P < 0.01$, Table 3). Furthermore, two critical time
457 points (135 min and 111 min) can be derived from the two fitted logarithmic equations, which
458 distinguished sediment deposition from sediment transport, signifying that the runoff began to
459 transport the deposited sediment on GB after 135 min and 111 min for 6.0 and 7.2 m³ h⁻¹ inflow
460 discharges.

461



462
463
464
465

Figure 10. Temporal variation in soil loss rate of the “upstream area—gully head—gully bed” system (a), upstream area (b), gully head (c) and gully bed (d)

Table 3. Relationships between soil loss rate of three landform units and time

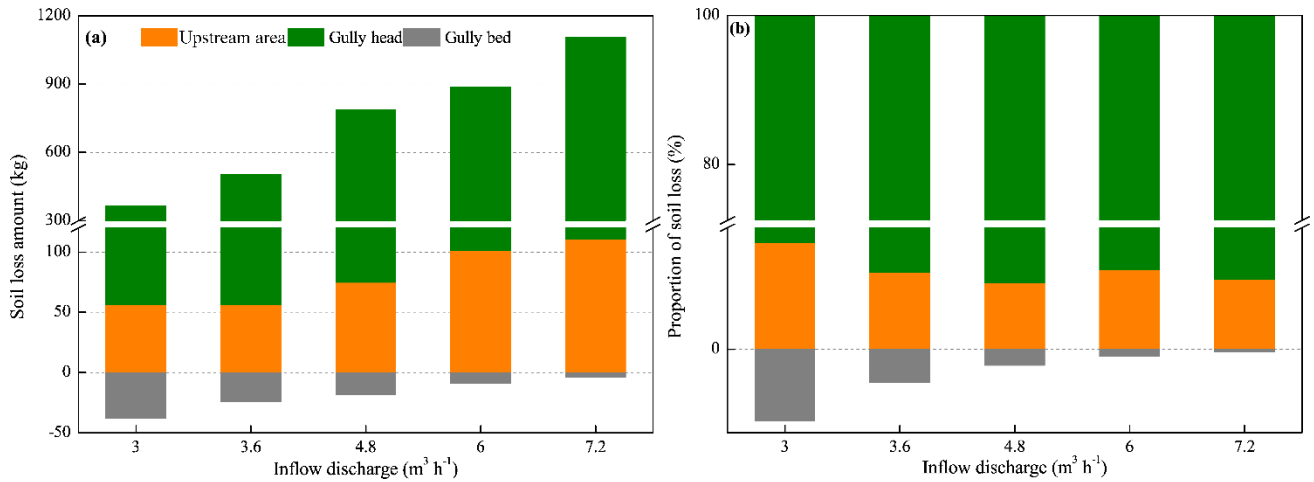
Inflow discharge (m ³ h ⁻¹)	Fitted equations		
	Upstream area	Gully head	Gully bed
3.0	$S_L = 15.71 - 2.34 \ln(t), R^2 = 0.909^{**}$	$S_H = 87.12 - 12.99 \ln(t), R^2 = 0.908^{**}$	$S_B = -182.62/t - 1.01, R^2 = 0.980^{**}$
3.6	$S_L = 23.97 - 4.18 \ln(t), R^2 = 0.938^{**}$	$S_H = 191.82 - 33.44 \ln(t), R^2 = 0.939^{**}$	$S_B = -64.46/t - 1.36, R^2 = 0.918^{**}$
4.8	$S_L = 28.76 - 4.85 \ln(t), R^2 = 0.930^{**}$	$S_H = 273.64 - 46.17 \ln(t), R^2 = 0.929^{**}$	$S_B = -109.36/t - 0.22, R^2 = 0.982^{**}$
6.0	$S_L = 44.0 - 7.69 \ln(t), R^2 = 0.884^*$	$S_H = 341.59 - 59.74 \ln(t), R^2 = 0.885^*$	$S_B = 2.03 \ln(t) - 9.96, R^2 = 0.936^{**}$
7.2	$S_L = 47.34 - 8.25 \ln(t), R^2 = 0.922^{**}$	$S_H = 425.24 - 74.07 \ln(t), R^2 = 0.924^{**}$	$S_B = 1.86 \ln(t) - 8.76, R^2 = 0.906^{**}$

466 Note: S_L , S_H and S_B are the soil loss rate of upstream area, gully head and gully bed, respectively. The sample No. is
467 6 for fitting equation. * and ** indicate the significant level of 0.05 and 0.01.

468 3.3.2 Spatial distribution of soil loss

469 The variation in soil loss amount and proportion of the three landform units (UA, GH, GB) with
470 inflow discharge is shown in Fig. 11. As illustrated in Fig. 11a, for the experiments of five inflow
471 discharges, the soil loss was dominant in the UA and GH, but the GB was dominated by sediment

472 deposition due to the weaker sediment transport capacity of runoff on GB than sediment deliverability
 473 of UA and GH. Furthermore, the soil loss amount of UA and GH ranged from 55.9 to 110.7 kg and
 474 from 310.0 to 994.8 kg, respectively, and increased linearly with increasing inflow discharge ($R^2 =$
 475 0.966 and 0.969, $P < 0.05$). The sediment deposition amount of GB ranged from 4.2 to 37.7 kg, and
 476 decreased with inflow discharge as a logarithmic function ($R^2 = 0.961$, $P < 0.05$). In terms of proportion
 477 of soil loss (Fig. 11b), the proportion of UA and GH reached the maximum (15.3%) and minimum
 478 (84.7%), respectively under $3.0 \text{ m}^3 \text{ h}^{-1}$ inflow discharge, whereas, the proportion exhibited a little
 479 change (UA: 9.5% - 11.4%; GH: 88.6% - 90.5%) when the inflow discharge is $7.2 \text{ m}^3 \text{ h}^{-1}$. Remarkably,
 480 the proportion of deposited sediment amount on GB to total soil loss amount ranged from 0.4% to
 481 10.3%, and decreased exponentially with inflow discharge ($R^2 = 0.992$, $P < 0.001$).



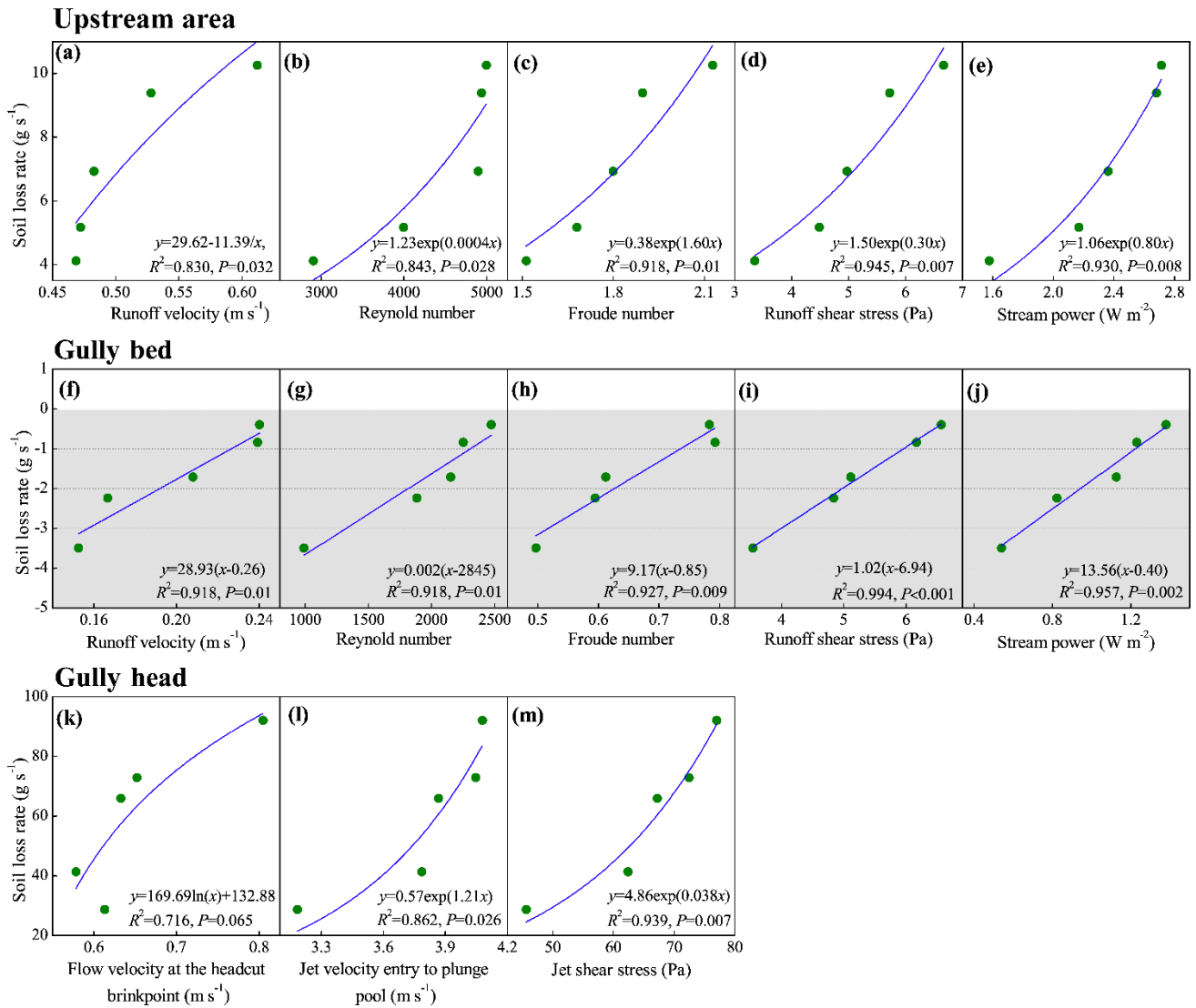
482
 483 **Figure 11.** Variation in soil loss amount (a) and proportion (b) of upstream area, gully head and gully bed with
 484 inflow discharge

485 3.4 Spatial change in hydrodynamic mechanism of soil loss

486 3.4.1 Relationships between soil loss and hydraulic parameters

487 Fig. 12 indicates the significant difference in the relationships between soil loss rate and hydraulic
 488 parameters among the three landform units (Fig. 12). For the upstream area (UA), the soil loss rate
 489 could be described as a series of exponential functions of runoff velocity, Reynold number, Froude
 490 number, runoff shear stress and stream power, of which the runoff shear stress and stream power had
 491 a closer correlation with soil loss (Fig. 12a - 12e, $R^2 = 0.830 - 0.945$). Furthermore, the increased speed
 492 of soil loss rate obviously increased with the increasing hydraulic parameters (except for runoff
 493 velocity), indicating that soil loss of UA showed a stronger sensitive response to increasing hydraulic

494 properties. However, the soil loss rate of gully bed (GB) linearly increased with the above-mentioned
 495 five parameters (Fig. 12f - 12j, $R^2 = 0.918 - 0.994$), which suggested that the decreased rate of sediment
 496 deposition of GB is basically constant with the increasing hydraulic properties. Further analysis
 497 showed that the critical runoff velocity, Reynold number, Froude number, runoff shear stress and
 498 stream power for triggering the transformation of sediment deposition to soil erosion on GB, and the
 499 critical values are 0.26 m s^{-1} , 2845, 0.85, 6.94 Pa and 0.40 W m^{-2} , respectively. For the gully head (GH)
 500 position, the soil loss was significantly affected by jet velocity entry to plunge pool and jet shear stress
 501 (Fig. 12l and 12m, $R^2 = 0.862$ and 0.939), while the relationship between soil loss and flow velocity at
 502 the headcut brink-point was not significant (Fig. 12k, $P = 0.065$).

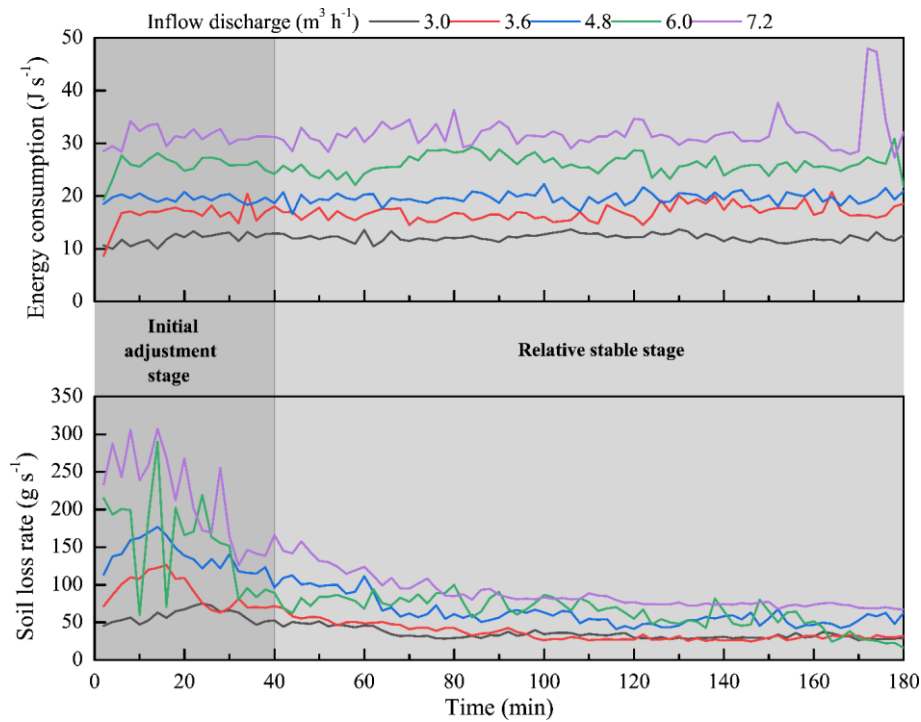


503
 504 **Figure 12.** Relationships between soil loss rate of upstream area, gully bed and gully head and runoff hydraulic and
 505 jet properties

506 3.4.2 Response of soil loss to energy consumption

507 The synchronous change of soil loss of “UA-GH-GB” system and total energy consumption can
508 be divided into two stages (Fig. 13). In the initial adjustment stage (0 - 40 min), the topsoil layer of
509 UA had the relative higher erodibility and was the main resource of soil loss, which caused the relative
510 lower flow velocity at the brinkpoint of gully head. Therefore, the most of flow discharge was
511 transformed as on-wall flow, so the most of flow energy consumed at the headwall. So, in this stage,
512 UA and gully headwall are the main positions of soil loss, and the most of flow energy was also
513 consumed in the two positions. With the gradual adjustment of upstream area morphology, the gully
514 erosion process entered into the relative stable stage (40 - 180 min). In this stage, the flow velocity at
515 headcut obviously increased and showed a slight change (Fig. 4a), and thus the headwall erosion and
516 plunge pool erosion also experienced a relative stable process. As a result, the soil loss and flow energy
517 consumption exhibited a similar change process. Occasionally, the occurrence of several gully head
518 and bank collapse events altered the synchronous change process of soil loss and energy consumption.

519 As illustrated in Fig. 14, on average, the soil loss rate of the “UA-GH-GB” system and the three
520 individual landform units was positively and significantly related to the energy consumption ($P < 0.05$),
521 and a logarithmic function was found to fit the relationship between soil loss rate and energy
522 consumption best ($R^2 = 0.889 - 0.987$). The critical energy consumption initiating the system is 7.53 J s^{-1}
523 (J s^{-1}) (Fig. 14a). Furthermore, there is critical energy consumption to initiate soil erosion of the upstream
524 area (UA) and gully head (GH) based on the fitted logarithmic functions (Fig. 14b, 14c). The critical
525 energy consumption for GH (5.79 J s^{-1}) is 2.57 times greater than that (1.62 J s^{-1}) of the UA. Similarly,
526 for the gully bed (Fig. 14d), the minimum energy consumption (1.64 J s^{-1}) is needed to trigger the
527 transformation of sediment deposition to soil loss. We found that the sum of critical energy
528 consumption initiating three landform units (9.05 J s^{-1}) was larger than the critical value initiating the
529 system, which was mainly attributed to the mass failure of gully head and bank inputting the additional
530 potential energy into the flow.

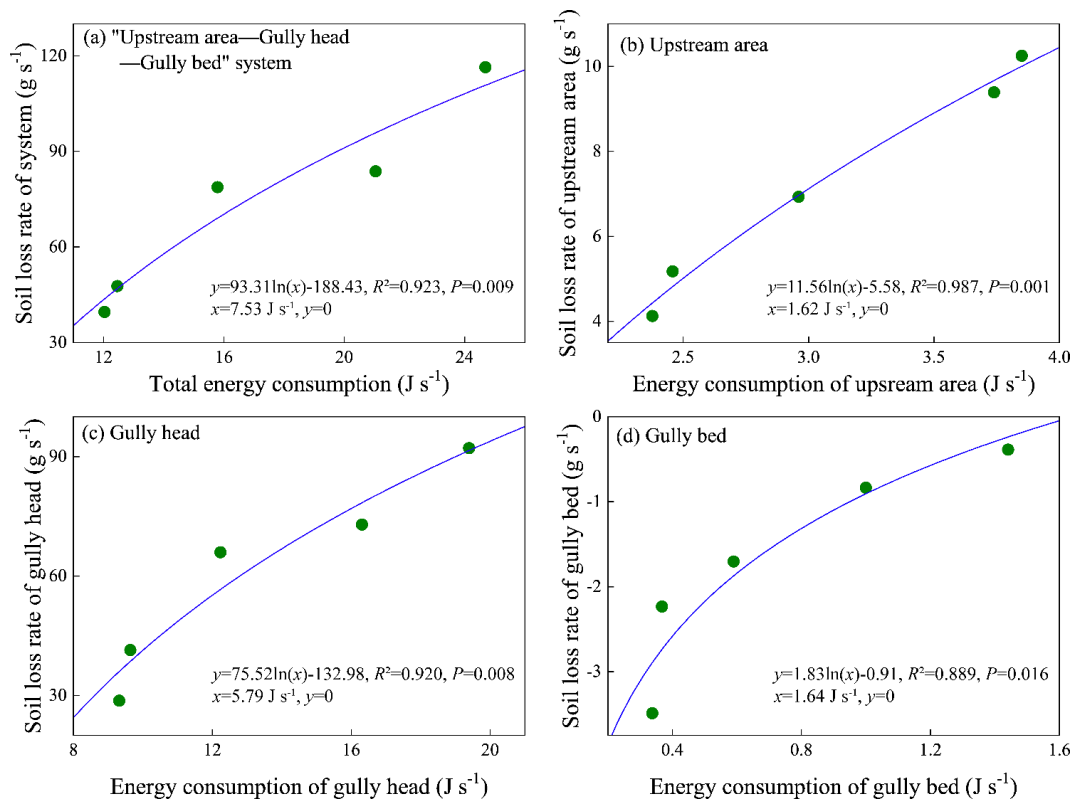


531

532

533

Figure 13. Synchronous change of soil loss rate of “upstream area-gully head-gully bed” system and total energy dissipation during headcut erosion



534

535

536

Figure 14. Relationships between soil loss rate of “upstream area-gully head-gully bed” system (a), upstream area (b), gully head (c) and gully bed(d) and energy consumption

537 4 Discussion

538 4.1 Spatial-temporal changes in hydraulic properties

539 This study showed that the runoff velocity at the headcut brink-point (V_b) firstly raised and then
540 gradually stabilized with experimental duration (Fig. 4a), which was closely corresponded to the
541 gradually decreased runoff width on the upstream area over time (Shi et al., 2020a). However, this
542 result was inconsistent with Zhang et al (2016, 2018) and Shi et al (2020b) who reported that the V_b
543 decreased over time, which was mainly due to the gradually increased roughness and resistance of
544 underlying surface over time reducing the runoff velocity in their studies (Battany and Grismer, 2015;
545 Su et al., 2015). The further analysis of power function between V_b and time ($V_b = a \cdot t^b$, Table 1) showed
546 that the a -value increased but the b -value showed a weak variation with the inflow discharge increased,
547 indicating that upstream flow discharge can improve initial V_b but not affect its change trend over time.
548 Therefore, we can extrapolate the erosion process and rule of upstream area from this simulation test
549 to the actual ground situation. By contrast, the jet velocity entry to plunge pool (V_e) and jet shear stress
550 (τ_j) experienced a gradually decreased process (Fig. 4c, 4e), which was mainly attributed to the fact
551 that the development of several second-headcut steps caused more energy consumption in plunge pools
552 and the lower potential energy at headcut brink-point due to the shortened jet flow height (Guo et al.,
553 2019; Jiang et al., 2020). This result, however, differed from the finding of Zhang et al. (2016) who
554 stated the V_e and τ_j remained stable as the experiments progressed, which was mainly attributed to the
555 weak change of jet-flow height induced by slow headcut retreat. This comparison manifested that the
556 jet flow properties was strongly determined by the headcut retreat process.

557 For the runoff hydraulic of upstream area (UA) and gully bed (GB), the Reynold number Re of
558 UA and GB initially increased and gradually stabilized, but the Froude number Fr showed an opposite
559 trend. This phenomenon was agreed with previous studies (e.g., Su et al., 2015; Zhang et al., 2016).
560 Besides, the Re and Fr of UA were larger than that of GB by 50.5% - 65.9% and 1.39 - 2.04 times,
561 respectively, under same inflow discharge upstream gully head, indicating that the runoff turbulence
562 became weaker after the runoff of UA passed the gully head and experienced plunge pool erosion (Shi
563 et al., 2020a). More evidently, the runoff on UA was in the supercritical-transition and supercritical-
564 turbulent flow regime ($Re > 500$, $Fr > 1$), whereas the runoff on GB belonged to subcritical-transition

565 and subcritical-turbulent flow regime ($Re > 500$, $Fr < 1$). However, Su et al. (2015) found that the
566 steady state Re of gully bed was higher than that of upstream area, which was mainly attributed to the
567 difference in slope gradient. In their study, the larger gully bed slope gradient than upstream area would
568 accelerate the runoff velocity and thus enhance flow turbulence (Bennett, 1999; Pan et al., 2016).
569 Furthermore, compared to UA, the τ and ω of GB increased and decreased by 2.8% - 15.7% and 49.2%
570 - 65.9%, respectively. The increased shear stress was caused by the decrease of flow velocity on gully
571 bed, and the drastically decreased stream power can reflect the energy consumption of flow for
572 transporting sediment on gully bed. This result was different from some previous experimental studies
573 on gully and bank gully under different conditions. Previous studies have proven that the lots of factors
574 including plunge pool size, slope gradient, initial step height, and soil texture influenced the hydraulic
575 properties from upstream area to gully bed is affected by various factors (Bennett and Casali, 2001;
576 Wells et al., 2009a, 2009b).

577 **4.2 Spatial-temporal change in runoff energy consumption and soil erosion**

578 Our study revealed that the accumulated runoff energy consumption of the upstream area (UA),
579 gully headcut (GH) and gully bed (GB) linearly increased over time (Fig. 8), indicating the spatial-
580 temporal change in energy consumption maintained a relatively steady state during gully headcut
581 erosion. However, the flow energy consumption of bank gully in three landform units logarithmically
582 increased over time (Su et al., 2015). This difference further manifested that the runoff energy
583 consumption of different landform units depends on gully type to some extent as well as soil texture,
584 slope and headwall height (Wells et al., 2009a). Besides, under this flow discharge conditions, the
585 proportion of energy consumption to the total flow energy ranged from 91.12% to 99.90%, indicating
586 that almost all of flow energy was consumed during headcut erosion. Furthermore, the proportion of
587 energy consumption in UA, GH and GB was 15.6% - 19.8%, 77.3% - 78.6% and 2.8% - 5.8%,
588 respectively (Fig. 9), which was also indirectly supported by the study of Su et al. (2015) who
589 suggested that the runoff energy consumption per unit soil loss from upstream area, headcut and gully
590 bed is 17.4%, 70.5% and 12.0%, respectively. This further signified that the gully head consumed the
591 most of runoff energy (77.5% on average) during headcut migration. The flow energy must be
592 consumed to surmount the soil resistance as headcut migrates, and the consumed energy was mainly

593 focused on headwall and plunge pool development (Alonso et al., 2002).

594 In terms of soil loss, our study indicated that the soil loss rate of the “UA-GH-GB” system initially
595 increased to the peak value and then gradually declined and stabilized (Fig. 10), which was consistent
596 with the results of many studies on rill and gully headcut erosion under different conditions (slope,
597 initial step height, flow discharge, soil type, soil stratification) (Bennett, 1999; Bennett and Casali,
598 2001; Gordon et al., 2007; Wells et al., 2009a; Shi et al., 2020a). Both the scour depth and sediment
599 production increased in the initial period of underlying surface adjustment, while once the plunge pool
600 development was maintained, and sediment yield decreased and gradually stabilized (Bennett et al.,
601 2000). In addition, the significant difference in soil loss process was found among the three landform
602 units. The soil loss of UA and GH decreased logarithmically over time, which was similar with several
603 studies (e.g., Su et al., 2015; Shi et al., 2020b). Nevertheless, the GB was always characterized by
604 sediment deposition for the inflow discharge of $< 4.8 \text{ m}^3 \text{ h}^{-1}$, whereas the sediment was deposited firstly
605 and then gradually transported as the inflow discharge increased to 6.0 and $7.2 \text{ m}^3 \text{ h}^{-1}$. Similar
606 phenomena were also found in some previous studies on rill headcut erosion (Bennett, 1999; Bennett
607 and Casali, 2001; Gordon et al., 2007; Wells et al., 2009a). This further indicated that soil
608 loss/deposition process of gully system was significantly influenced by three landform units, and
609 especially, the most of flow energy (77.5%) consumed at gully heads due to jet flow erosion strongly
610 weakened sediment transport capacity of flow on gully bed and thus changed the soil loss/deposition
611 process of gully system. However, Su et al. (2014, 2015) revealed a larger soil loss volume or soil loss
612 rate in gully bed than upstream area and headwall during bank gully headcut erosion. This difference
613 between our study and Su et al. (2014, 2015) is primarily caused by the difference in slope gradient.
614 The gully bed slope (20°) of bank gully was larger than that (3°) of our study, indicating the runoff on
615 gully bed of bank gully had stronger sediment transport capacity (Zhang et al., 2009; Ali et al., 2013;
616 Wu et al., 2016, 2018). Besides, some previous also proved that the soil type, surface roughness, slope-
617 length, groundwater/surface runoff were the main factors influencing soil loss by gully erosion (Amare
618 et al., 2020; Li et al., 2021). In view of the proportion of soil loss, the proportion of UA and GH was
619 9.5% - 11.4% and 88.6% - 90.5%, respectively, of which the proportion of deposited sediment on GB
620 to the sediment yield from UA and GH can reach up to 0.4% - 10.3%. This result fully demonstrated

621 that the gully head is the main source of sediment production during gully headcut erosion (Oostwoud-
622 Wijdenes & Bryan, 1994; Zhao, 1994; Su et al., 2014), and also manifested the necessary and
623 importance of gully headcut erosion controlling in gully-dominated region (Amare et al., 2019).

624 **4.3 Hydrodynamic characteristics of headcut erosion**

625 The significantly different relationships between soil loss and jet or hydraulic characteristics were
626 found among UA, GH, and GB. The soil loss rate of UA exponentially increased with five hydraulic
627 parameters (runoff velocity, Reynold number, Froude number, runoff shear stress and stream power),
628 indicating that soil loss of UA showed a stronger sensitive response to increasing hydraulic properties.
629 This could attribute to the frequent bank collapse on UA accelerating soil loss (Wells et al., 2013; Qin
630 et al., 2018). However, the sediment deposition rate of GB linearly decreased with the five hydraulic
631 parameters, signifying that sediment deposition on GB decreased at a stable state with the increase of
632 hydraulic parameters. Therefore, the sediment deposition rate would reach zero when the five
633 hydraulic parameters increased to the critical values, implying that the transformation of sediment
634 deposition to sediment transport on GB would be triggered. Furthermore, the shear stress is the optimal
635 parameter describing soil loss process of UA and GB, which differed from some studies on
636 hillslope/gully erosion hydrodynamic characteristics (Zhang et al., 2009; Shen et al., 2019; Ma et al.,
637 2020; Sidorchuk, 2020). Most of studies have verified that stream power is the superior hydrodynamic
638 parameter describing soil detachment process. This comparison also fully illustrated the great
639 difference in hydrodynamic characteristic between hillslope erosion and headcut erosion. In this study,
640 the soil loss of gully head (including plunge pool erosion) was significantly affected by jet properties.
641 It's confirmed that the plunge pool erosion by jet flow becomes a crucial process controlling gully
642 head migration and sediment production (Oostwoud-Wijdenes et al., 2000). Consequently, the plunge
643 pool erosion theory is usually employed to build several headcut retreat models (Alonso et al., 2002;
644 Campo-Bescós et al., 2013). Although the weak correlation between soil loss of gully head and flow
645 velocity at headcut breakpoint, the larger flow velocity resulted from increasing inflow discharge
646 would improve the shear stress of jet flow impinging gully bed, and thus the gully headcut suffered
647 stronger incisional erosion of the plunge pool. However, in fact, the soil loss of gully head was also
648 affected by on-wall flow erosion (Chen et al., 2013; Guo et al., 2021a), and thus more studies should

649 be conducted to clear the effect of on-wall flow properties on headwall erosion.

650 From the energy consumption perspective, the soil loss rate of the three landform units
651 significantly and logarithmically increased with the energy consumption, and the similar change trend
652 was also found in the study of Su et al. (2015). This finding suggests that energy consumption could
653 be considered as the available parameter to estimate the soil loss of gully headcut erosion (Shi et al.,
654 2020b). Furthermore, we found the critical energy consumption initiating soil erosion of UA, GH, and
655 GB are 1.62 J s^{-1} , 5.79 J s^{-1} and 1.64 J s^{-1} , respectively, indicating the soil loss of gully head (including
656 plunge pool) needs more flow energy consumption (Zhang et al., 2018; Shi et al., 2020a, 2020b). This
657 phenomenon can be attributed to the fact that the more runoff energy was consumed at the gully
658 headwall and plunge pool erosion than UA and GB and thus resulted in more severe soil loss during
659 headcut erosion. In addition, we found that the critical energy consumption activating soil loss of “UA-
660 GH-GB” system was lower the sum of critical energy consumption initiating soil loss and sediment
661 transport of three landform units (9.05 J s^{-1}). This result was closely related to mass failures such as
662 gully head and gully bank collapse can contribute the additional energy into the flow. So, the role of
663 gravitational erosion in controlling gully erosion process should be clarified in the future studies.

664 **5 Implication, significance and limitations of this study**

665 Gully erosion has been studied for nearly a century, but its process and dynamic mechanism are
666 still difficult to clearly understand and reveal. Given this, our study attempted to clarify the spatial-
667 temporal changes in flow hydraulic characteristics, energy consumption and soil loss and expound the
668 response of soil loss to runoff properties and energy consumption during headcut erosion through a
669 series of simulation experiment under controlled conditions. These results could be extended to wider
670 conditions, such as gully scale, flow discharge determined by rainfall and drainage area, which can
671 promote the understanding of process and mechanism of gully erosion under real ground conditions
672 as well as the modelling and prediction of gully erosion. Especially, the variation and proportion of
673 energy consumption along “UA-GH-GB” in the process of gully erosion and its influence on sediment
674 yield were clearly elucidated in this study, which has an important guiding significance for gully
675 erosion control practice and restoration efforts. We can design some engineering and/or vegetation
676 measures at gully heads to pre-consume the most flow energy and the energy dissipation structures

677 could be designed and installed at the position where plunge pool develops. Also, the appropriate size
678 of these measures also can be determined to ensure the flow energy of different landform units was
679 lower than the corresponding critical energy consumption.

680 However, there are some potential limitations in our study. First, considering the complex effects
681 of lots of factors on gully erosion, the flow discharge upstream gully heads was designed as the core
682 factor affecting gully erosion in our study, and the five levels of flow discharge was generated
683 according to the rainfall, landform and gully morphology. But it is not really same as the actual ground
684 situations, such as the flow discharge upstream gully heads would not be constant during a rainfall
685 event. Second, it has not been confirmed how well our experimental results are in line with the actual
686 ground results. Therefore, further studies need to verify the experimental results with the actual
687 situations, so that the study results can be practiced and applied under actual rainfall conditions. Third,
688 in the future research, gully erosion experiments under different control measures should be carried
689 out to identify suitable gully erosion prevention measures. Although the earlier-noted imperfection
690 represents the limitation of our study, we still clearly demonstrated the temporal-spatial change in
691 hydraulic properties and soil loss during headcut erosion and quantify the response relationships of
692 soil loss of different landform units to energy consumption, which is of great significance for
693 deepening the understanding of the gully process and hydrodynamic mechanism. Also, our results can
694 provide valuable ideas and scientific basis for the construction of gully erosion model and the design
695 of gully erosion prevention measures.

696 **Summary**

697 This study investigated the temporal-spatial changes in flow hydraulic, energy consumption and
698 soil loss during headcut erosion based on a series of scouring experiments of gully headcut erosion.
699 The temporal changes in jet properties of gully head (GH) were significantly affected by upstream
700 inflow discharge. The upstream area (UA) and gully bed (GB) had similar temporal changes in
701 Reynold number, Froude number, shear stress and stream power. The flow was supercritical on UA,
702 but subcritical on GB, and the turbulent degree was enhanced by the increasing inflow discharge. The
703 presence of gully headwall significantly weakened flow Reynold number, shear stress and stream
704 power, but lightly enhanced the Froude number. The accumulated energy consumption at UA, GH and

705 GB linearly increased with time. Overall, more than 91% of total flow energy was consumed during
706 headcut erosion, of which the GH accounted for 77.5% of the total runoff energy dissipation. The soil
707 loss of UA and GH decreased logarithmically over time, whereas the GB was mainly characterized by
708 sediment deposition over time. The GH and UA contributed 88.5% and 11.5% of total soil loss,
709 respectively, of which 3.8% soil loss was deposited on GB. The soil loss process of UA and GH and
710 the sediment deposition process of GB were significantly affected by flow hydraulic and jet properties.
711 Our results revealed that the critical runoff energy consumption to initiate soil erosion of UA, GH and
712 GB are 1.62 J s^{-1} , 5.79 J s^{-1} and 1.64 J s^{-1} , respectively. The runoff energy consumption should be
713 considered as a non-negligible parameter to predict gully headcut erosion.

714 **Data availability**

715 The data that support the findings of this study are available from the first author
716 (guomingming@iga.ac.cn) and corresponding author upon request (nwafu_wwl@163.com).

717 **Author contribution**

718 Mingming Guo and Wenlong Wang designed the experiments. Mingming Guo, Zhuoxin Chen,
719 Tianchao Wang, Qianhua Shi, Man Zhao and Lanqian Feng carried out the experiments. Zhuoxin Chen
720 produced and processed the digital elevation model of erosion landform. Mingming Guo and
721 Wennlong Wang written and prepared the manuscript with contributions from all co-authors.

722 **Competing interests**

723 The authors declare that they have no conflict of interest.

724 **Acknowledgments**

725 This work was supported by the National Natural Science Foundation of China (42077079,
726 41571275), the China Postdoctoral Science Foundation (2020M681062, 2021T140663), and the
727 National Key Research and Development Program of China (2016YFC0501604).

728 **References**

- 729 Addisie, M.B., Ayele, G.K., Gessess, A.A., Tilahun, S.A., Zegeye, A.D., Moges, M.M., ... Steenhuis, T.S.: Gully
730 head retreat in the sub-humid Ethiopian Highlands: The Ene-Chilala catchment, *Land Degradation &*
731 *Development*, 28, 1579–1588, <https://doi.org/10.1002/ldr.2688>, 2017.
- 732 Ali, M., Seeger, M., Sterk, G., Moore, D.: A unit stream power based sediment transport function for overland
733 flow. *Catena*. 101, 197-204. <https://doi.org/10.1016/j.catena.2012.09.006>
- 734 Alonso, C.V., Bennett, S.J., Stein, O.R., 2002. Predicting head cut erosion and migration in concentrated flows
735 typical of upland areas, *Water Resources Research*, 38, 39-1–39-15, <http://dx.doi.org/10.1029/2001WR001173>,
736 2013.
- 737 Amare, S., Keesstra, S., van der Ploeg, M., Langendoen, E., Steenhuis, T., Tilahun, S.: Causes and controlling
738 factors of Valley bottom Gullies. *Land*, 8(9), 141, <https://doi.org/10.3390/land8090141>, 2019.
- 739 Amare, S., Langendoen, E., Keesstra, S., Ploeg, M. V. D., Gelagay, H., Lemma, H., van der Zee, S. E.:
740 Susceptibility to Gully Erosion: Applying Random Forest (RF) and Frequency Ratio (FR) Approaches to a Small
741 Catchment in Ethiopia. *Water*, 13(2), 216, <https://doi.org/10.3390/w13020216>, 2021.
- 742 Arabameri, A., Chen, W., Lombardo, L., Blaschke, T., Tien Bui, D.: Hybrid computational intelligence models
743 for improvement gully erosion assessment, *Remote Sensing*, 12(12), <https://doi.org/10.3390/rs12010140>, 140,
744 2020.
- 745 Battany, M.C., Grismer, M.E.: Rainfall runoff and erosion in Napa Valley vineyards: effects of slope, cover and
746 surface roughness, *Hydrological Processes*, 14(7), 1289-1304, [https://doi.org/10.1002/\(SICI\)1099-
747 1085\(200005\)14:7<1289::AID-HYP43>3.0.CO;2-R](https://doi.org/10.1002/(SICI)1099-1085(200005)14:7<1289::AID-HYP43>3.0.CO;2-R), 2015.
- 748 Beer, C.E., Johnson, H.P.: Factors in gully growth in the deep loess area of western Iowa. *Transactions of ASAE*,
749 6, 237–240, <https://doi.org/10.13031/2013.40877>, 1963.
- 750 Belayneh, M., Yirgu, T., Tsegaye, D.: Current extent, temporal trends, and rates of gully erosion in the Gumara
751 watershed, northwestern Ethiopia, *Global Ecology and Conservation*, 24, e01255,
752 <https://doi.org/10.1016/j.gecco.2020.e01255>, 2020.
- 753 Bennett, S.J., Casali, J.: Effect of initial step height on headcut development in upland concentrated flows. *Water*
754 *Resources Research*, 37, 1475–1484, <https://doi.org/10.1029/2000WR900373>, 2001.
- 755 Bennett, S.J.: Effect of slope on the growth and migration of headcuts in rills, *Geomorphology*, 30, 273–290,
756 [https://doi.org/10.1016/S0169-555X\(99\)00035-5](https://doi.org/10.1016/S0169-555X(99)00035-5), 1999.
- 757 Bennett, S.J., Alonso, C.V.: Turbulent flow and bed pressure within headcut scour holes due to plane reattached
758 jets, *Journal of Hydraulic Research*, 44, 510–521, <https://doi.org/10.1080/00221686.2006.9521702>, 2006.
- 759 Bennett, S.J., Alonso, C.V., Prasad, S.N., Romkens, M.J.: Experiments on headcut growth and migration in
760 concentrated flows typical of upland areas, *Water Resources Research*, 36, 1911–1922,
761 <https://doi.org/10.1029/2000WR900067>, 2000.
- 762 Bogale, A. G., Aynalem, D. W., Adem, A. A., Mekuria, W., Tilahun, S.: Spatial and temporal variability of soil
763 loss in gully erosion in upper Blue Nile basin, Ethiopia, *Applied Water Science*, 10(5), 106,
764 <https://doi.org/10.1007/s13201-020-01193-4>, 2020.
- 765 Campo-Bescós, M.A., Flores-Cervantes, J.H., Bras, R.L., Casali, J., Giráldez, J.V.: Evaluation of a gully headcut
766 retreat model using multitemporal aerial photographs and digital elevation models, *Journal of Geophysical*
767 *Research: Earth Surface*, 118, 2159–2173, <https://doi.org/10.1002/jgrf.20147>, 2013.

768 Chaplot, V., Giboire, G., Marchand, P., Valentin, C.: Dynamic modelling for linear erosion initiation and
769 development under climate and land-use changes in northern Laos, *Catena*, 63, 318–328,
770 <https://doi.org/10.1016/j.catena.2005.06.008>, 2005.

771 Che, X.L.: Study of distribution characteristic and evolution of headward erosion on Dongzhi tableland of the
772 loess gully region, Yangling: Northwest A&F University, pp. 66-67, (In Chinese), 2012.

773 Chen, A., Zhang, D., Peng, H., Fan, J., Xiong, D., Liu, G.: Experimental study on the development of collapse
774 of overhanging layers of gully in Yuanmou Valley, China, *Catena*, 109, 177-185,
775 <https://doi.org/10.1016/j.catena.2013.04.002>, 2013.

776 De Baets, S., Poesen, J., Knapen, A., Galindo, P.: Impact of root architecture on the erosion-reducing potential
777 of roots during concentrated flow, *Earth Surface Processes and Landforms*, 32, 1323–1345,
778 <https://doi.org/10.1002/esp.1470>, 2007.

779 de Vente, J., Poesen, J.: Predicting soil erosion and sediment yield at the basin scale: Scale issues and semi-
780 quantitative models, *Earth-Science Reviews*, 71, 95–125, <https://doi.org/10.1016/j.earscirev.2005.02.002>, 2005.

781 DeLong, S.B., Johnson, J., Whipple, K.: Arroyo channel head evolution in a flash-flood-dominated
782 discontinuous ephemeral stream system, *Geological Society of America Bulletin*, 126, 1683–1701,
783 <https://doi.org/10.1130/B31064.1>, 2014.

784 Descroix, L., González Barrios, J.L., Viramontes, D., Poulénard, J., Anaya, E., Esteves, M., Estrada, J.: Gully
785 and sheet erosion on subtropical mountain slopes: their respective roles and the scale effect, *Catena*, 72, 325–
786 339, <https://doi.org/10.1016/j.catena.2007.07.003>, 2008.

787 Dotterweich, M., Rodzik, J., Zglobicki, W., Schmitt, A., Schmidtchen, G., Bork, H.R.: High resolution gully
788 erosion and sedimentation processes, and land use changes since the Bronze Age and future trajectories in the
789 Kazimierz Dolny area (Nałęczów Plateau, SE-Poland), *Catena*, 95, 50–62,
790 <https://doi.org/10.1016/j.catena.2012.03.001>, 2012.

791 Flores-Cervantes, J., Istanbuluoglu, E., Bras, R.: Development of gullies on the landscape: A model of headcut
792 retreat resuUAing from plunge pool erosion, *Journal of Geophysical Research*, 111, 1–14,
793 <https://doi.org/10.1029/2004JF000226>, 2006.

794 Frankl, A., Stal, C., Abraha, A., Nyssen, J., Rieke-Zapp, D., DeWulf, A., Poesen, J.: Detailed recording of gully
795 morphology in 3D through image-based modelling, *Catena*, 127, 92–101,
796 <https://doi.org/10.1016/j.catena.2014.12.016>, 2015.

797 Fu, B.J., Liu, Y., Lv, Y.H., He, C.S., Zeng, Y., Wu, B.F.: Assessing the soil erosion control service of ecosystems
798 change in the Loess Plateau of China, *Ecological Complexity*, 8, 284-293,
799 <https://doi.org/10.1016/j.ecocom.2011.07.003>, 2011.

800 Gordon, L.M., Bennett, S.J., Wells, R.R., Alonso, C.V.: Effect of soil stratification on the development and
801 migration of headcuts in upland concentrated flows, *Water Resources Research*, 43, W07412,
802 <https://doi.org/10.1029/2006WR005659>, 2007.

803 Guo, M., Wang, W., Shi, Q., Chen, T., Kang, H., Li, J.: An experimental study on the effects of grass root density
804 on gully headcut erosion in the gully region of China's Loess Plateau, *Land Degradation & Development*, 30,
805 2107–2125, <https://doi.org/10.1002/ldr.3404>, 2019.

806 Guo, M., Wang, W., Wang, T., Wang, W., Kang, H.: Impacts of different vegetation restoration options on gully
807 head soil resistance and soil erosion in loess tablelands, *Earth Surface Processes and Landforms*, 45(4), 1038-
808 1050, <https://doi.org/10.1002/esp.4798>, 2020a.

809 Guo, M.M., Wang, W.L., Kang, H.L., Yang, B.: Changes in soil properties and erodibility of gully heads induced
810 by vegetation restoration on the Loess Plateau, China, *Journal of Arid Land*, 10(5), 712-725,
811 <https://doi.org/10.1007/s40333-018-0121-z>, 2018.

812 Guo, M.M., Wang, W.L., Li, J.M., Bai, Y., Kang, H.L., Yang, B.: Runoff characteristics and soil erosion dynamic
813 processes on four typical engineered landforms of coalfields: An in-situ simulated rainfall experimental study,
814 *Geomorphology*, 349, 106896, <https://doi.org/10.1016/j.geomorph.2019.106896>, 2020b.

815 Guo, M.M., Lou, Y.B., Chen, Z.X., Wang, W.L., Feng, L.Q., Zhang, X.Y.: The proportion of jet flow and on-
816 wall flow and its effects on soil loss and plunge pool morphology during gully headcut erosion, *Journal of*
817 *Hydrology*, 598, 126220, <https://doi.org/10.1016/j.jhydrol.2021.126220>, 2021a.

818 Guo, M.M., Chen, Z.X., Wang, W.L., Wang, T.C., Wang, W.X., Cui, Z.Q.: Revegetation induced change in soil
819 erodibility as influenced by slope situation on the Loess Plateau, *Science of the Total Environment*, 772, 145540,
820 <https://doi.org/10.1016/j.scitotenv.2021.145540>, 2021b.

821 Hager, W.H.: Hydraulics of plane free overfall, *Journal of Hydraulic Engineering*, 109, 1683–1697,
822 [https://doi.org/10.1061/\(ASCE\)0733-9429\(1983\)109:12\(1683\)](https://doi.org/10.1061/(ASCE)0733-9429(1983)109:12(1683)), 1983.

823 Hanson, G.J., Robinson, K.M., Cook, K.R.: Prediction of headcut migration using a deterministic approach,
824 *Transactions of the ASAE*, 44(4), 525-531, <https://doi.org/10.13031/2013.6112>, 2001.

825 Hosseinalizadeh, M., Kariminejad, N., Chen, W., Pourghasemi, H.R., Alinejad, M., Behbahani, A.M.,
826 Tiefenbacher, J.P.: Gully headcut susceptibility modeling using functional trees, naïve Bayes tree, and random
827 forest models, *Geoderma*, 342, 1-11, <https://doi.org/10.1016/j.geoderma.2019.01.050>, 2019.

828 Ionita, I.: Gully development in the Moldavian Plateau of Romania, *Catena*, 68, 133–140,
829 <https://doi.org/10.1016/j.catena.2006.04.008>, 2006.

830 Ionita, I., Niacsu, L., Petrovici, G., Blebea-Apostu, A.M.: Gully development in eastern Romania: a case study
831 from Falciu Hills, *Natural Hazards*, 79, 113–138, <https://doi.org/10.1007/s11069-015-1732-8>, 2015.

832 Jiang, Y., Shi, H., Wen, Z., Guo, M., Zhao, J., Cao, X., Fan, Y., Zheng, C.: The dynamic process of slope rill
833 erosion analyzed with a digital close range photogrammetry observation system under laboratory conditions,
834 *Geomorphology*, 350, 106893, <https://doi.org/10.1016/j.geomorph.2019.106893>, 2020.

835 Jiao, J.Y., Wang, W.Z., Hao, X.P.: Precipitation and erosion characteristics of rainstorm in different pattern on
836 Loess Plateau, *Journal of Arid Land Resources and Environment*, 13(1), 34-42, (In Chinese), 1999.

837 Kirkby, M.J., Bull, L.J., Poesen, J., Nachtergaele, J., Vandekerckhove, L.: Observed and modelled distributions
838 of channel and gully heads—with examples from SE Spain and Belgium, *Catena*, 50, 415–434,
839 [https://doi.org/10.1016/S0341-8162\(02\)00128-5](https://doi.org/10.1016/S0341-8162(02)00128-5), 2003.

840 Li, Binbing., Huang, Lei., Feng, Lin., Li, Peng., Yao, Jingwei., Liu, Fangming., Li, Junli., Tang, Hui.: Gully
841 sidewall expansion process on loess hill slope erosion, *Journal of Basic Science and Engineering*, 24(6), 1147-
842 1158. (In Chinese), 2016.

843 Li, H., Cruse, R.M., Liu, X.B., Zhang, X.Y.: Effects of topography and land use change on gully development
844 in typical Mollisol region of Northeast China, *Chinese Geographical Science*, 26, 779-788,
845 <https://doi.org/10.1007/s11769-016-0837-7>, 2016.

846 Li, M., Song, X.Y., Shen, B., Li, H.Y., Meng, C.X.: Influence of vegetation change on producing runoff and
847 sediment in gully region of Loess Plateau, *Journal of Northwest Sci-Tech University of AgricuUAure and*
848 *Forestry (Natural Science Edition)*, 34, 117-120, (In Chinese), 2006.

849 Li, Y., Mo, Y. Q., Are, K. S., Huang, Z., Guo, H., Tang, C., Abegunrin, T.P., Qin, Z.H, Kang, Z.W., Wang, X.:
850 Sugarcane planting patterns control ephemeral gully erosion and associated nutrient losses: Evidence from

851 hillslope observation. *Agriculture, Ecosystems & Environment*, 309, 107289,
852 <https://doi.org/10.1016/j.agee.2020.107289>, 2021.

853 Li, Z., Zhang, Y., Zhu, Q., He, Y., Yao, W.: Assessment of bank gully development and vegetation coverage on
854 the Chinese Loess Plateau, *Geomorphology*, 228, 462–469, <https://doi.org/10.1016/j.geomorph.2014.10.005>,
855 2015.

856 Li, Z., Zheng, F.L., Liu, W.Z., Flanagan, D.C.: Spatial distribution and temporal trends of extreme temperature
857 and precipitation events on the Loess Plateau of China during 1961–2007, *Quaternary International*, 226(1-2),
858 92-100, <https://doi.org/10.1016/j.quaint.2010.03.003>, 2010.

859 Ma, Q., Zhang, K., Cao, Z., Wei, M., & Yang, Z.: Soil detachment by overland flow on steep cropland in the
860 subtropical region of China, *Hydrological Processes*, 34(8), 1810-1820, <https://doi.org/10.1002/hyp.13694>,
861 2020

862 Martínez-Casasnovas, J.A., Concepción Ramos, M., García-Hernández, David.: Effects of land - use changes
863 in vegetation cover and sidewall erosion in a gully head of the Penedès region (northeast Spain), *Earth Surface*
864 *Processes & Landforms*, 34, 1927-1937, <https://doi.org/10.1002/esp.1870>, 2009.

865 Nazari Samani, A., Ahmadi, H., Mohammadi, A., Ghoddousi, J., Salajegheh, A., Boggs, G., Pishyar, R.: Factors
866 Controlling Gully Advancement and Models Evaluation (Hableh Rood Basin, Iran), *Water Resources*
867 *Management*, 24, 1532–1549, <https://doi.org/10.1007/s11269-009-9512-4>, 2010.

868 Oostwoud-Wijdenes, D., Bryan, R.B.: The significance of gully headcuts as a source of sediment on low-angle
869 slopes at Baringo, Kenya, and initial control measures, *Advances in Geocology*, 27, 205–231, 1994.

870 Oostwoud-Wijdenes, D., Poesen, J., Vandekerckhove, L., Ghesquiere, M.: Spatial distribution of gully head
871 activity and sediment supply along an ephemeral channel in a Mediterranean environment, *Catena*, 39, 147–
872 167, [http://202.194.143.28:80/rwt/SD/https/MSYXTLUQPJUB/10.1016/S0341-8162\(99\)00092-2](http://202.194.143.28:80/rwt/SD/https/MSYXTLUQPJUB/10.1016/S0341-8162(99)00092-2), 2000.

873 Pan, C., Ma, L., Wainwright, J., Shanguan, Z.: Overland flow resistances on varying slope gradients and
874 partitioning on grassed slopes under simulated rainfall, *Water Resources Research*, 52, 2490–2512,
875 <https://doi.org/10.1002/2015WR018035>, 2016.

876 Poesen, J., Nachtergaele, J., Verstraeten, G., Valentin, C.: Gully erosion and environmental change: Importance
877 and research needs, *Catena*, 50, 91-133, [https://doi.org/10.1016/S0341-8162\(02\)00143-1](https://doi.org/10.1016/S0341-8162(02)00143-1), 2003.

878 Qin, Chao., Zheng, Fenli., Wells Robert, R., Xu, Ximeng, Wang, Bin., Zhong, Keyuan.: A laboratory study of
879 channel sidewall expansion in upland concentrated flows, *Soil and Tillage Research*, 178, 22-31,
880 <https://doi.org/10.1016/j.still.2017.12.008>, 2018.

881 Reuter, H.I., Nelson, A., Jarvis, A.: An evaluation of void filling interpolation methods for SRTM data,
882 *International Journal of Geographic Information Science*, 21(9), 983-1008, 2007.

883 Rieke-Zapp, D.H., Nichols, M.H.: Headcut retreat in a semiarid watershed in the southwestern United States
884 since 1935, *Catena*, 87, 1–10, <https://doi.org/10.1016/j.catena.2011.04.002>, 2011.

885 Rodzik, J., Furtak, T., Zglobicki, W.: The impact of snowmelt and heavy rainfall runoff on erosion rates in a
886 gully system, Lublin Upland, Poland, *Earth Surface Processes & Landforms*, 34, 1938–1950,
887 <https://doi.org/10.1002/esp.1882>, 2009.

888 Rouse, H.: *Engineering hydraulics*. Hoboken, NJ: Wiley, 1950.

889 Sanchis, M.P., Torri, D., Borselli, L., Poesen, J.: Climate effects on soil erodibility, *Earth Surface Processes &*
890 *Landforms*, 33, 1082–1097, <https://doi.org/10.1002/esp.1604>, 2008.

891 Shen, N., Wang, Z., Zhang, Q., Chen, H., Wu, B.: Modelling soil detachment capacity by rill flow with hydraulic
892 variables on a simulated steep loessial hillslope, *Hydrology Research*, 50(1), 85-98,
893 <https://doi.org/10.2166/nh.2018.037>, 2018.

894 Shi, Q.H., Wang, W.L., Guo, M.M., Chen, Z.X., Feng, L.Q., Zhao, M., Xiao, H.: The impact of flow discharge
895 on the hydraulic characteristics of headcut erosion processes in the gully region of the Loess Plateau,
896 *Hydrological processes*, 34, 718-729, <https://doi.org/10.1002/hyp.13620>, 2020.

897 Shi, Q., Wang, W., Zhu, B., Guo, M.: Experimental study of hydraulic characteristics on headcut erosion and
898 erosional response in the tableland and gully regions of China, *Soil Science Society of America Journal*, 84,
899 700–716, <https://doi.org/10.1002/saj2.20068>, 2020.

900 Sidorchuk, A.: The potential of gully erosion on the Yamal peninsula, West Siberia. *Sustainability*, 12(1), 260,
901 <https://doi.org/10.3390/su12010260>, 2020.

902 Stein, O., Julien, P., Alonso, C.: Mechanics of jet scour downstream of a headcut, *Journal of Hydraulic Research*,
903 31, 723–738, <https://doi.org/10.1080/00221689309498814>, 1993.

904 Su, Z.A., Xiong, D.H., Dong, Y.F., Zhang, B.J., Zhang, S., Zheng, X.Y., Fang, H.D.: Hydraulic properties of
905 concentrated flow of a bank gully in the dry - hot valley region of southwest China, *Earth Surface Processes
906 and Landforms*, 40, 1351 - 1363. <https://doi.org/10.1002/esp.3724>, 2015.

907 Su, Z.A., Xiong, D.H., Dong, Y.F., Li, J.J., Yang, D., Zhang, J.H., He, G.X.: Simulated headward erosion of
908 bank gullies in the Dry-hot Valley Region of southwest China, *Geomorphology*, 204, 532–541,
909 <https://doi.org/10.1016/j.geomorph.2013.08.033>, 2014.

910 Sun, W.Y., Mu, X.M., Song, X.Y., Wu, D., Cheng, A.F., Qiu, B.: Changes in extreme temperature and
911 precipitation events in the Loess Plateau (China) during 1960–2013 under global warming, *Atmospheric
912 Research*, 168, 33-48, <https://doi.org/10.1016/j.atmosres.2015.09.001>, 2016.

913 Thompson, J.R.: Quantitative effect of watershed variables on rate of gully - head advancement. *Transactions
914 of the ASABE*, 7, 54 - 55, <https://doi.org/10.13031/2013.40694>, 1964.

915 Torri, D., Poesen, J.: A review of topographic threshold conditions for gully head development in different
916 environments, *Earth-Science Reviews*, 130, 73–85, <https://doi.org/10.1016/j.earscirev.2013.12.006>, 2014.

917 Valentin, C., Poesen, J., Li, Y.: Gully erosion: Impacts, factors and control, *Catena*, 63, 132–153,
918 <https://doi.org/10.1016/j.catena.2005.06.001>, 2005.

919 Vandekerckhove, L., Poesen, J., Govers, G.: Medium-term gully headcut retreat rates in southeast Spain
920 determined from aerial photographs and ground measurements, *Catena*, 50(2-4), 329-352,
921 [https://doi.org/10.1016/S0341-8162\(02\)00132-7](https://doi.org/10.1016/S0341-8162(02)00132-7), 2003.

922 Vandekerckhove, L., Poesen, J., Wijdenes, D.O., Nachtergaele, J., Tomás de Figueiredo.: Thresholds for gully
923 initiation and sedimentation in Mediterranean Europe, *Earth Surface Processes & Landforms*, 25(11), 1201-
924 1220, [https://doi.org/10.1002/1096-9837\(200010\)25:11<1201::AID-ESP131>3.0.CO;2-L](https://doi.org/10.1002/1096-9837(200010)25:11<1201::AID-ESP131>3.0.CO;2-L), 2015.

925 Vanmaercke, M., Poesen, J., Mele, B.V., Demuzere, M., Bruynseels, A., Golosov, V., Yermolaev, O.: How
926 fast do gully headcuts retreat?, *Earth - Science Reviews*, 154, 336 - 355,
927 <https://doi.org/10.1016/j.earscirev.2016.01.009>, 2016.

928 Vannoppen, W., Vanmaercke, M., De Baets, S., Poesen, J.: A review of the mechanical effects of plant roots on
929 concentrated flow erosion rates, *Earth - Science Reviews*, 150, 666 - 678,
930 <https://doi.org/10.1016/j.earscirev.2015.08.011>, 2015.

931 Vanwalleghem, T., Bork, H.R., Poesen, J., Schmidtchen, G., Dotterweich, M., Nachtergaele, J., Bork, H.,
932 Deckers, J., Brüsich, B., Bungeneers, J., De Bie, M.: Rapid development and infilling of a buried gully under
933 cropland, Central Belgium, *Catena*, 63, 221–243, <https://doi.org/10.1016/j.catena.2005.06.005>, 2005.

934 Vanwalleghem, T., Van Den Eeckhaut, M., Poesen, J., Deckers, J., Nachtergaele, J., Van Oost, K., Slenters, C.:
935 Characteristics and controlling factors of old gullies under forest in a temperate humid climate: a case study
936 from the Meerdaal Forest (Central Belgium), *Geomorphology*, 56(1), 15–29, <https://doi.org/10.1016/S0169-937>
937 555X(03)00043-6, 2003.

938 Wells, R.R., Alonso, C.V., Bennett, S.J.: Morphodynamics of Headcut Development and Soil Erosion in Upland
939 Concentrated Flows, *Soil Science Society of America Journal*, 73, 521–530.
940 <https://doi.org/10.2136/sssaj2008.0007>, 2009a.

941 Wells, R.R., Bennett, S.J., Alonso, C.V.: Effect of soil texture, tailwater height, and pore - water pressure on the
942 morphodynamics of migrating headcuts in upland concentrated flows, *Earth Surface Processes and Landforms*,
943 34, 1867 - 1877, <https://doi.org/10.1002/esp.1871>, 2009b.

944 Wells, R.R., Momm, H.G., Rigby, J.R., Bennett, S.J., Bingner, R.L., Dabney, S.M.: An empirical investigation
945 of gully widening rates in upland concentrated flows, *Catena*, 101, 114-121,
946 <https://doi.org/10.1016/j.catena.2012.10.004>, 2013.

947 Wen, X., Wu, X., Gao, M.: Spatiotemporal variability of temperature and precipitation in Gansu province
948 (northwest China) during 1951–2015, *Atmospheric Research*, 197, 132-149,
949 <https://doi.org/10.1016/j.atmosres.2017.07.001>, 2017.

950 Wen, Y., Kasielke, T., Li, H., Zhang, B., Zepp, H.: May agricultural terraces induce gully erosion? a case study
951 from the black soil region of northeast China. *Science of The Total Environment*, 750(4), 141715,
952 <https://doi.org/10.1016/j.scitotenv.2020.141715>, 2020.

953 Wu, Bing., Wang, Zhanli., Zhang, Qingwei., Shen, Nan., Liu, June., Wang, Sha.: Evaluation of shear stress and
954 unit stream power to determine the sediment transport capacity of loess materials on different slopes, *Journal of*
955 *Soil & Sediments*, 18, 116–127, <https://doi.org/10.1007/s11368-017-1758-5>, 2018.

956 Wu, B., Wang, Z., Shen, N., Wang, S.: Modelling sediment transport capacity of rill flow for loess sediments on
957 steep slopes, *Catena*, 147, 453-462, <https://doi.org/10.1016/j.catena.2016.07.030>, 2016.

958 Xia, L., Song, X.Y., Fu, N., Li, H.Y., Li, Y.L.: Impacts of land use change and climate variation on green water
959 in the Loess Plateau Gully Region—A case study of Nanxiaohegou basin, *Journal of Hydraulic Engineering*,
960 48(6), 678-688, (In Chinese), 2017.

961 Xu, J.Z., Li, H., Liu, X.B., Hu, W., Yang, Q.N., Hao, Y.F., Zhen, H.C., Zhang, X.Y.: Gully Erosion Induced by
962 Snowmelt in Northeast China: A Case Study, *Sustainability*, 11, <https://doi.org/10.3390/su11072088>, 2019.

963 Xu, X.M., Zheng, F.L., Wilson, G.V., Wu, M.: Upslope inflow, hillslope gradient and rainfall intensity impacts
964 on ephemeral gully erosion, *Land Degradation & Development*, 28, 2623-2635 <https://doi.org/10.1002/ldr.2825>,
965 2017.

966 Xu, X.M., Zheng, F.L., Qin, C., Wu, H.Y., Wilson, G.V.: Impact of cornstalk buffer strip on hillslope soil erosion
967 and its hydrodynamic understanding, *Catena*, 149, 417–425, <https://doi.org/10.1016/j.catena.2016.10.016>, 2017.

968 Xu, X.M., Wang, H.B., Zhao, J.Y., Liu, X.J.: Dynamic variation of soil erosion of Nanxiaohegou small
969 watershed during 2004-2016, *Soil and Water Conservation in China*, 443(2), 59-61, (In Chinese), 2019.

970 Yang, C.T.: Potential energy and stream morphology, *Water Resource Research*, 7(2), 311-223,
971 <https://doi.org/10.1029/WR007i002p00311>, 1971a.

972 Yang, C.T.: On river meanders, *Journal of Hydrology*, 13, 231-253, <https://doi.org/10.1016/0022->
973 1694(71)90226-5, 1971b.

974 Zhang, B.J., Xiong, D.H., Su, Z.A., Yang, D., Dong, Y.F., Xiao, L., Zhang, S., Shi, L.T.: Effects of initial step
975 height on the headcut erosion of bank gullies: a case study using a 3D photo-reconstruction method in the Dry-
976 hot Valley region of southwest China, *Physical Geography*, 37, 409–429,
977 <https://doi.org/10.1080/02723646.2016.1219939>, 2016.

978 Zhang, B.J., Xiong, D.H., Zhang G.H., Zhang, S., Wu, H., Yang, D., Xiao, L., Dong, Y.F., Su, Z.A., Lu, X.N.:
979 Impacts of headcut height on flow energy, sediment yield and surface landform during bank gully erosion
980 processes in the Yuanmou Dry - hot Valley region, southwest China, *Earth Surface Processes & Landforms*,
981 43(10), 2271-2282, <https://doi.org/10.1002/esp.4388>, 2018.

982 Zhang, H.X.: The characteristics of hard rain and its distribution over the Loess Plateau, *Acta Geographica*
983 *Sinica*, 38, 416–425, (In Chinese), 1983.

984 Zhang, G.H., Liu, Y.M., Han, Y.F., Zhang, X.C.: Sediment transport and soil detachment on steep slopes: I.
985 transport capacity estimation, *Soil Science Society of America Journal*, 73, 1291-1297,
986 <https://doi.org/10.2136/sssaj2008.0145>, 2009.

987 Zhang, X., Fan, J., Liu, Q., Xiong D.: The contribution of gully erosion to total sediment production in a small
988 watershed in Southwest China, *Physical Geography*, 39(3), 1-18,
989 <https://doi.org/10.1080/02723646.2017.1356114>, 2018.

990 Zhao, A.C.: Analysis of control models of typical small watershed in gully area of Loess Plateau, the east part
991 of Gansu Province, *Research of Soil and Water Conservation*, 1, 45–49, (In Chinese), 1994.

992 Zhu, T.X.: Gully and tunnel erosion in the hilly Loess Plateau region, China, *Geomorphology*, 153, 144–155,
993 <https://doi.org/10.1016/j.geomorph.2012.02.019>, 2012.